Modelling Short Crack Propagation under Variable Structural and Thermal Loadings

Alexander Bosch[1]
Michael Vormwald[2]
[1]Department of Materials Technology, MTU Aero Engines AG, Munich, Germany
[2]Materials Mechanics Group, Technische Universität Darmstadt, Darmstadt, Germany

Correspondence
Alexander Bosch, Department of Materials Technology, MTU Aero Engines AG, Dachauer Str. 665, 80995 Munich, Germany. Email: alexander.bosch@mtu.de

Funding information
Arbeitsgemeinschaft industrieller Forschungsvereinigungen „Otto von Guericke“ e.V. (AiF) within the scope of the program for advancement of the industrial alliance of research (IGF) of the Federal Ministry for Economic Affairs and Energy (BMWi) on the basis of a decision by the German Bundestag.

ABSTRACT
Concepts for crack propagation as well as fatigue assessment under variable mechanical and thermal loadings are unestablished. For variable mechanical loadings, the damage parameter P_J is well known, for thermal loadings the damage parameter D_TMF is established. Both parameters base on the effective cyclic J-Integral, still the definition is different. The damage parameters P_J considers the effective stress and strain ranges from the upper reversal point of each load cycle to the point of crack closure. Depending on the loading sequence the point of crack closure is treated as a history variable. In addition, with a crack length dependant fatigue limit, the most important sequence effects are considered. A new P_J-based concept is developed by considering additional sequence effects. In comparison to experimental results, the developed concept is able to reduce scattering in the range of constant amplitude loading tests.

KEYWORDS
J-integral, short-crack growth, crack propagation, thermo-mechanical fatigue

1 | INTRODUCTION

Due to the increasing use of renewable energies, power plants are operated more and more flexibly. The originally stationary operation, which was only interrupted by shutdowns and commissioning for regular inspections, has become a demand-oriented operation. By this operation mode, the additional load is expressed in a high number of smaller load changes. The

load cycles themselves are mainly induced by temperature changes. The guidelines for the design and assessment of such components (e.g. KTA3201.2[1] or ASME Code Section VIII[2]) focus on the evaluation of the thermomechanical start-stop cycle. The resulting elastic-plastic strain amplitudes clearly assign the stress situation to the low cycle fatigue (LCF) regime. Further, important factors influencing the fatigue life of the components such as the mean stresses, the sequence effects in case of variable amplitude loading or also the influence of the component's size are covered rather generally by providing the Wöhler line for the strain amplitudes with corresponding factors. Against the background of this initial situation, manufacturers and operators of power plants (with any kind of power generation) have an increased need for a more realistic assessment of the fatigue life under service loads. The request goes so far that the calculation method is online capable and shows the corresponding danger potential in the context of a power plant monitoring. The actors involved are aware that, especially in the presence of possibly large plastic deformations, load sequence effects occur which lead to much shorter lifetimes than those calculated with the classical Palmgren[3]-Miner[4] rule. This linear damage accumulation rule assumes under variable amplitude loading, that the frequency n_i of cycles at load level i causes a numerical contribution to the damage sum normalising n_i by the number of cycles to failure N_i under constant amplitude loading. The damage sum contributions are supposed to add up linearly:

$$D = \sum_{i=1}^{k} \frac{n_i}{N_i}. \tag{1}$$

As for constant amplitude loading, the failure damage sum is assumed to be $D = 1.0$.
The greatest shortcoming of this rule is that the sequence of the occurring stress and strain cycles cannot be considered, although this has a very large influence on the lifetime. To be able to display sequence effects at all, the material element and with it, the mechanically loaded component must be able to store information about the load history. In the field of mechanics, there are only two possible memory storages for load histories, plastic deformation and material separation[5]. Nevertheless, the task of sequence recording in the damage accumulation calculation has not yet been fully solved. The present special issue with contributions to the fourth conference on Variable Amplitude Loading is an eloquent testimony of ongoing research activities on this topic. It is beyond the intention of this paper to give a comprehensive overview of the damage accumulation problem. The still current overviews of Fatemi and Yang[6] and Skorupa[7,8] give a first insight into the matter.
The first step in determining the influence of the plastic deformation history on service life is to simulate it for the potential locations of technical crack initiation. The local strain approach is available for this purpose. Dowling[9] has compiled its elements. The German Research Association for Mechanical Engineers has published a comprehensive set of rules for standardized

application (FKM guideline nonlinear)[10,11]. The approach presented here follows this guideline in its basic version; extensions and further developments are introduced where appropriate. The guideline[11] specifies damage parameter life curves for assessing fatigue lives to technical crack initiation. One of the two parameters, P_{RAJ}, is derived from the cyclic J-integral. The origin of this parameter goes back to Vormwald and Seeger[12], there still under the name P_J. The procedure assumes the existence of a short crack, whose growth rate is linked to the cyclic J-integral by a power law. The sequence effects were captured realistically by including a history variable for the crack opening strains in the simulation of the elastic-plastic stress-strain path. An adjustment of mean stress sensitivities and size effects was done in later publications[13,14]. In the guideline[11] the fatigue life calculation is transferred from an integration of the crack growth rate to a damage accumulation calculation of the Palmgren-Miner type. In the present paper, this is discarded.

The developed concepts, considering mean stresses and load history as well as the temperature dependency individually on the load side, is based on the P_J-concept. Improvements are made by substituting of the crack propagation law and performing a crack propagation calculation instead of a damage accumulation. Further improvements are made for the modelling of the transition of the threshold for small cracks to long cracks and the consideration of transient crack closure. The concepts variants differ in the crack propagation law and the consideration of transient crack closure in style of Anthes[15], but all of them can be applied even under variable temperatures. All concept variants share the relatively easy identification of the required parameters, which are to be determined mainly using results of constant amplitude loading and static tension tests. The advantages of the improvements and the fracture mechanics based approaches are shown in contrast to the results of conventional approaches. The developed concept is discussed in connection with additional load sequence effects. The present paper is an extended version of the paper published in the proceedings of the fourth Conference on Variable Amplitude Loading[16].

2 | EXPERIMENTAL CAMPAIGN

2.1 | Material

In a joint research project, the experimental investigations[17,18] focussed on the metastable austenitic stainless steel X6CrNiNb18-10. It is a commonly used steel for components of pressurised components of light water reactors in Germany. In this project a variety of models were developed for assessing variable amplitude fatigue under isothermal as well as thermomechanical loading conditions. After the end of the project some models were further developed. The paper at hand presents the current state of model development and the results of the lifetime calculations achievable with it. A presentation of all details, the reproduction of which would go beyond the scope of this paper, can also be found in the monograph by Bosch[19].

Many austenitic steels show a plasticity induced phase transformation when mechanically loaded at room temperature[20,21]. The material investigated here does not make an exception. However, the maximum operating temperature of the components of interest is about ~370°C. While a phase transformation from austenite to martensite is observed at room temperature, this phenomenon does not occur under higher temperatures. Especially, when temperature variations between 50°C and 370°C were applied as done in the present investigation, the formation of martensite could not be observed. For most of the isothermal experiments performed, a temperature of 180°C was chosen, which is the mean temperature in operation.

2.2 | Specimens

A variety of different specimens tested. From a scientific point of view, it is desirable to separate the sequence effects from the size effects. For this reason, a large number of experiments were carried out on almost unnotched material specimens, which are shown in Fig. 1 as hourglass, smooth, weld or Gleeble specimens. The notation IWM indicates that the experiments have been performed in the laboratory of the research partner Fraunhofer Institute of Materials Mechanics, Freiburg, IFSW states that the test were done in the laboratory of the authors. The specimens labelled “Gleeble” have undergone temperature-time sequences as they were measured in the heat-affected zone (HAZ) of the weld specimens during the weld process. The tests on notched and welded specimens are intended to show that the findings on variable amplitude life calculation obtained on unnotched specimens can also be used to evaluate the structural durability of components.

Notched and welded specimens are characterized by a stress concentration factor of $K_\mathrm{t} = 1.57$ and $K_\mathrm{t} = 3.0$, respectively, both associated with the net section nominal stress and determined by a FE-Analyses. Mainly due to the statistic size effect, their notch fatigue factors are reduced to $K_\mathrm{f} = 1.26$ and $K_\mathrm{f} = 1.93$. The constant amplitude life curves were calculated by applying the local strain approach in connection with the material’s life curve, the notch approximation procedure by Neuber[22] and an adjusted fixing of the notch fatigue factors. Considering the statistical size effect would have provided nearly the same numbers.

2.3 | Constant amplitude loading

Results of strain-controlled constant amplitude loading tests ($R_\varepsilon = -1$) are in good comparison with data from literature (eg. KTA 3201.2[1]), for LCF as well as for HCF. The stress responses at half lifetime $(N/2)$ were used to determine the parameters for the cyclic stress-strain curve. The cyclic hardening coefficient and exponent as used in the Ramberg-Osgood[23] equation are $K' = 1121\ \mathrm{MPa}$ and $n' = 0.2309$ (temperature is 180°C). Young’s modulus was determined at this temperature to $E = 183000\ \mathrm{MPa}$. Based on force-controlled constant amplitude loading tests of the hourglass-specimens at 180°C, the endurance limit up to a limit load cycle of $N =$

$2 \cdot 10^6$, was determined to $\sigma_D = 214\ \mathrm{MPa}$, using the method of Probits[24]. The corresponding strain is $\varepsilon_D = 0.194\%$.

Due to the process of welding, the heat input up to a temperature of 1200°C for the weld-specimens in the heat affected zone (HAZ) and the simulated HAZ of the Gleeble-specimens, leads to a recrystallization of the microstructure. As a result of a subsequent slow cooling in air, the grains have more time to grow. The larger grain sizes even affect the strength, resulting in a lower measurable hardness. For the hourglass-specimens, the hardness was determined to >200 HV10, for the HAZ of the weld-specimens and the Gleeble-specimens, the hardness was measured about ~140 HV1. In the consequence, the transferability is not given. Therefore, the endurance limit for the Gleeble- and Weld-specimens was estimated to $\sigma_D = 160\ \mathrm{MPa}$.

As observed by the hysteresis loops under constant amplitude loading, the austenitic steel X6CrNiNb18-10 shows a strong Non-Masing-behaviour. This is also known as 'strain range effect'[25], with an increased loading the material hardens isotropically by an increasing yield strength. Simultaneously the kinematic plastic deformation behaviour equals more and more an ideal plastic behaviour at the reversal points. Incremental formulated plasticity models, like the models from Döring[26] and Fang[27], can describe the evolution of isotropic and kinematic hardening. Against the background of the increased effort in processing, this possibility was not further pursued.

2.4 | Variable amplitude loading

In the application relevant here, the variable mechanical load is caused by temperature changes of the medium carried along. Therefore, the operators of such plants monitor the temperature variations over time and calculate the local stress-time histories. Framatome GmbH gave the results of a plant shut down for a piping at a critical area (welded flange). After rainflow counting, the frequency distribution of the cycles was approximated by superposing two Gaussian-like spectra - Sum of two Gaussian like distributed load spectra (SoftGild). The spectrum contents are 100 cycles for the high amplitude spectrum and 10000 cycles otherwise, see Fig. 2.

For the experimental investigations by block and pseudo-random loading tests, the spectrum was divided into 8 steps, each which the same step size. In the block-tests or eight-stages tests, the cycles are run in ascending and descending order, while the individual cycles for the service loading tests are randomized (but with same sequence for each test). Fig. 2 shows the spectrum for both the eight stages and the pseudo-random load. The maximum nominal applied strain amplitude was chosen for those tests was chosen to 0.5% or 0.7%. In some of the pseudo-random load tests of the Gleeble- and weld-specimens a thermocycle between 50°C and 350°C was superposed. The frequency of the thermocycle is much lower than frequency of the structural loading. One thermocycle corresponds to an average of 112 load cycles for

welded specimens and an average of 80 load cycles for Gleeble-specimens. In the consequence, the thermal conditions for each mechanical cycle can be seen as isothermal, but over time the thermal condition is non isothermal.

These tests are complemented by two stage tests at 180°C, where one big cycle is followed by 10, 100, 1000 or 10000 small cycles. The amplitudes of the latter may be above or below the initial endurance limit. The maximum nominal applied strain amplitude was chosen for HG specimens to 1.0% and 1.5%, for notched specimen to 1.0% and for weld and Gleeble-specimens to 0.5% and 0.7%.

All tests under variable amplitude loadings have in common that the biggest cycles are always performed under a strain ratio of $R_\varepsilon = -1$. The smaller cycles are hung either at its upper reversal point (Fig. 3, column A) or its lower reversal point (Fig. 3, column C). This leads to high tensile or compressive mean stresses of the small cycles. The positioning on the descending branch of the hysteresis loop of the large cycle under $R_\varepsilon = -1$ (Fig. 3, column B) leads to moderate compressive mean stresses.

A total of 124 variable amplitude loading test results are available for the validation of any life calculation model.

As observed under constant amplitude loading, the strange range effect also occurs under variable amplitude loading. Fig. 4 shows a comparison between measured and calculated stress amplitudes over mean stresses for eight stage and pseudo-random loading tests each with the condition of constant upper and lower reversal points in strain. Calculations were performed by the Masing-Memory behaviour with the Ramberg-Osgood law based on the defined load-spectra. The experimentally monitored cycles show lower mean stresses as well as lower stress amplitudes than calculated. Deviations through lower stress amplitudes for the highest loadings result mainly by the reversibility of the described strain range effect. Deviations in mean stress result mainly by accumulated mean stress relaxation. Especially with higher plastic deformations mean stress relaxation is induced. Higher scattering of mean stresses for pseudo-random loading than for the eight stage tests concerning the lowest amplitude level can be explained by the left variable reversal point of the previous load cycle. Deviations of too low amplitudes concerning the lowest amplitude under pseudo-random loading are owned by control technology of the servo hydraulic testing machine.

3 | CRACK PROPAGATION MODEL

3.1 | Isothermal fatigue

Describing the metal fatigue phenomenon by modelling crack growth is an ongoing effort for six decades. Numerous researchers have contributed. Again, it is beyond the scope of this paper to give an overview. Only the latest version of a model development which started in the early 1990s[12,13] and was re-vitalised, recently[17,19,28–30]. However, it should be noted that the

ideas used in the authors' models are not unique. Especially the models of the IWM[31–35] (based on Heitmann's[36,37] damage parameter Z_{D}) follow similar approaches and lead to comparable results. Only the publications of Kamaya and Kawakubo[38] and the school around Topper[39]shall be additionally mentioned here.

Only the variant leading to the best comparison between calculated and experimental fatigue life is presented in this paper: PJ-RifoT2. This variant will be mainly compared in the following to the original P_{J}-concept: PJ-Orig[40]. The designations PJ-Orig and PJ-RifoT2 are chosen as in an earlier monograph for reasons of consistency.

An approximate solution for the effective cyclic J-Integral is applied according to Dowling[41], for half-circular surface crack in half-space. The damage parameter P_{J} considers sequence effects by taking the effective stress- and strain-ranges into account, which vary depending on the sequence under variable amplitude loading. Another considered sequence effect depends on the crack length, caused by the decreasing fatigue strength with increasing crack length. The transition from short crack growth to long crack growth is only considered by the threshold behaviour, the additional higher crack growth rate of short cracks is considered integrally over the whole fatigue life. The developed concept variant PJ-RifoT2 differs from PJ-Orig at first by the crack propagation law:

$$\frac{\mathrm{d}a}{\mathrm{d}n} = \begin{cases} C_{\mathrm{J}} \cdot (\Delta J_{\mathrm{eff}})^{m_{\mathrm{J}}} & \text{for } \Delta J_{\mathrm{eff}} \geq \Delta J_{\mathrm{eff,th}} \quad \text{PJ-Orig} \quad (2) \\ C_{\mathrm{J}} \cdot \left((\Delta J_{\mathrm{eff}})^{m_{\mathrm{J}}} - \left(\Delta J_{\mathrm{eff,th}}\right)^{m_{\mathrm{J}}}\right) & \text{for } \Delta J_{\mathrm{eff}} \geq \Delta J_{\mathrm{eff,th}} \quad \text{PJ-RifoT2} \quad (3) \end{cases}$$

Eq. (2) can be integrated analytically with $P_{\mathrm{J}} = \Delta J_{\mathrm{eff}}/a = \mathrm{const.}$ from initial crack length a_0 to crack length at failure a_{end}:

$$N = \frac{(a_{\mathrm{end}})^{1-m_{\mathrm{J}}} - (a_0)^{1-m_{\mathrm{J}}}}{(1-m) \cdot C_{\mathrm{J}}} \cdot \left(P_{\mathrm{J}}\right)^{-m_{\mathrm{J}}}. \quad (4)$$

This leads to an explicit relation between actual crack length a and relative damage n/N by:

$$n/N = \frac{(a)^{1-m_{\mathrm{J}}} - (a_0)^{1-m_{\mathrm{J}}}}{(a_{\mathrm{end}})^{1-m_{\mathrm{J}}} - (a_0)^{1-m_{\mathrm{J}}}}. \quad (5)$$

Based on this relation, in the original P_{J}-concept a linear damage accumulation is performed rather than a crack growth calculation. Using Eq. (3), a crack growth calculation has to be performed for PJ-RifoT2 instead of a linear damage accumulation and the crack growth rate is a function of the effective cyclic J-Integral. Considering the threshold value $\Delta J_{\mathrm{eff,th}}$ in the crack growth law results in a load dependent behaviour for relation between crack length and relative damage n/N under constant amplitude loading, see Fig. 5. This requires an improved approach to identify the crack growth parameters C_{J} and m_{J}, based on constant amplitude loading tests. Therefore, only fatigue tests were considered, where the influence of the threshold value $\Delta J_{\mathrm{eff,th}}$ is neglectable: $P_J = \Delta J_{\mathrm{eff}}/a \gg \Delta J_{\mathrm{eff,th}}/a$. Only tests with lifetimes lower than 10000 cycles were chosen. For this case, Eq. (3) can be treated as Eq. (2), with the benefit to calculate the fatigue life analytically according to Eq. (4). To consider the threshold behaviour of short

cracks similarly as El Haddad[42] or Tanaka[43], the integration limits are to be extended by the microstructural length l^*:

$$N = \frac{\left(\left(a_{\mathrm{end}} + l^*\right)\right)^{1-m_{\mathrm{J}}} - \left(\left(a_0 + l^*\right)\right)^{1-m_{\mathrm{J}}}}{\left(1 - m_{\mathrm{J}}\right) \cdot C_{\mathrm{J}}} \cdot \left(P_{\mathrm{J}}\right)^{-m_{\mathrm{J}}} = Q \cdot \left(P_{\mathrm{J}}\right)^{-m_{\mathrm{J}}}. \tag{6}$$

For the identification of the parameter Q and the crack growth exponent m_{J}, a P_{J}-Wöhler-curve needs to be fitted by a linear regression to the pairs of lifetimes $N(< 10000\ \mathrm{cyc.})$ and P_{J} with:

$$P_{\mathrm{J}} = \frac{\Delta J_{\mathrm{eff}}}{a} = \left[1.24 \frac{\Delta\sigma_{\mathrm{eff}}{}^2}{E} + \frac{1.02}{\sqrt{n'}} \Delta\sigma_{\mathrm{eff}} \cdot \left(\Delta\varepsilon_{\mathrm{eff}} - \frac{\Delta\sigma_{\mathrm{eff}}}{E}\right)\right]. \tag{7}$$

Therefore, the effective stress and strain ranges $\Delta\sigma_{\mathrm{eff}}$ and $\Delta\varepsilon_{\mathrm{eff}}$ are calculated between the difference of the upper reversal point of the hysteresis loop and the point of crack closure:

$$\Delta\sigma_{\mathrm{eff}} = \sigma_{\mathrm{max}} - \sigma_{\mathrm{cl}}, \tag{8}$$

$$\Delta\varepsilon_{\mathrm{eff}} = \varepsilon_{\mathrm{max}} - \varepsilon_{\mathrm{cl}}. \tag{9}$$

The crack opening stress is calculated according to Newman's model[44], under the assumption that the crack opening strain is equal to the crack closure strain $\varepsilon_{\mathrm{op}} = \varepsilon_{\mathrm{cl}}$. With the identified parameter Q and the crack growth exponent m_{J}, the additional parameters like the initial crack length a_0 and the microstructural length l^* as well as the crack growth constant C_{J} can now be identified. At this step, the additional consideration of transient crack closure plays an important role as an improvement in contrast to the original P_{J}-concept. Under constant amplitude loading, the original P_{J}-concept uses a constant stabilized crack closure strain, independent from crack length. Transient crack closure means, that the crack closure stress develops with the increasing crack length under constant amplitude loading, too. With this additional component in the concept, the fact is taken into account, that the stabilized level of plasticity induced crack closure still has to be formed. At the beginning of crack initiation by forming slip bands, the crack growths along those slip bands in a direction of 45° to the loading as a shear crack (Stage I)[45,46]. At this state, growth of those cracks is very sensitive to microstructure by grain boundaries, triple points, and phase boundaries[47–49]. During shear crack growth no plasticity induced crack closure effects are active and the whole cycle of each hysteresis loop is fully damaging[15]. The crack closure effect only sets in with the transition to Modus I cracks (Stage II) at higher stresses and/or longer cracks. The influence of transient crack closure on the effective stress and strain ranges is very important in the HCF regime. In the LCF regime the effective stress and strain ranges are approximately equal to the full stress and strain ranges, so that $P_{\mathrm{J}} = const.$ under constant amplitude loading and Eq. 4 can still be used. The transient crack closure strain is formulated under the conditions of constant amplitude loadings by:

$$\varepsilon^{a}_{\mathrm{cl,const}} = \varepsilon_{\mathrm{cl,const}} - \left(\varepsilon_{\mathrm{cl,const}} - \varepsilon_{\mathrm{min}}\right) \cdot \exp\left(\left(a - a_0\right)/\Delta a_{\mathrm{ref}}\right). \tag{10}$$

The delay constant Δa_{ref} is not only used for modelling the transient crack closure behaviour. Anthes[15] showed that under variable amplitude loading, the transition between a current crack

closure strain $\varepsilon_{\mathrm{cl}}$ and a stabilized crack closure strain $\varepsilon^{\mathrm{a}}_{\mathrm{cl,const}}$ can be expressed in the same way:

$$\varepsilon_{\mathrm{cl,new}} = \varepsilon^{\mathrm{a}}_{\mathrm{cl,const}} - \left(\varepsilon^{\mathrm{a}}_{\mathrm{cl,const}} - \varepsilon_{\mathrm{cl}}\right) \cdot \exp(-\Delta a/\Delta a_{\mathrm{ref}}). \tag{11}$$

Anthes[15] describes his delay parameter according to Gamache and McEvily[50] as rezobroke dependency on the ultimate tensile strength R_{m} by:

$$\Delta a_{\mathrm{ref}} = \frac{\mathrm{MPa} \cdot \mathrm{mm}}{R_{\mathrm{m}}} \cdot \frac{872}{90}. \tag{12}$$

The difference between damage contributions according to older (PJ-Orig) and updated crack incrementally controlled delay (PJ-RifoT2) is shown for an example of a two stage test in Fig. 6. In the older version, the delay occurs identically in each run through the load spectrum. Based on crack length controlled delay, in the first runs through the load spectra, the effective strain ranges of the smaller cycles are not reduced and their amplitudes are damaging with their full range. Only with a higher crack length and longer crack increments, the crack opening strain exceeds minimum strain of the individual cycles. Vormwald as well as Anthes used for evaluation of their delay constant. The delay constant Δa_{ref} was derived by theoretical considerations and validations[19] using Prestrain-Wöhler-curves from Heuler[51]:

$$\Delta a_{\mathrm{ref}} = \left(\frac{38.8\mathrm{MPa}}{R_{\mathrm{m}}} \cdot \left((0.25\mathrm{mm} + \mathrm{a}_0^* - a_0)^{1-m_{\mathrm{J}}} - (a_0^*)^{1-m_{\mathrm{J}}}\right) + (a_0^*)^{1-m_{\mathrm{J}}}\right)^{\frac{1}{1-m_{\mathrm{J}}}} - a_0^* \tag{13}$$

with

$$a_o^* = \frac{\Delta J_{\mathrm{eff,th}}}{P_{\mathrm{J,D}}^{a=a_0}}. \tag{14}$$

Thereby, $P_{\mathrm{J,D}}^{a=a_0}$ denotes the initial value for the P_{J}-parameter at the level of the endurance limit, calculated by the full stress and strain ranges $\Delta\sigma_{\mathrm{D}}$ and $\Delta\varepsilon_{\mathrm{D}}$:

$$P_{\mathrm{J,D}}^{a=a_0} = \left[1.24\frac{{\Delta\sigma_{\mathrm{D}}}^2}{E} + \frac{1.02}{\sqrt{n'}}\Delta\sigma_{\mathrm{D}} \cdot \left(\Delta\varepsilon_{\mathrm{D}} - \frac{\Delta\sigma_{\mathrm{D}}}{E}\right)\right], \tag{15}$$

while the threshold of the effective cyclic J-Integral $\Delta J_{\mathrm{eff,th}}$ is kept independent from R-ratio and is approximately calculated by the Young's modulus based on data from Taylor[52] with:

$$\Delta J_{\mathrm{eff,th}} = \frac{E}{5 \cdot 10^6}\,\mathrm{mm}. \tag{16}$$

The presented effective threshold is to be interpreted as an intrinsic value. The proposed delay constant, Eq. (13), yields much smaller values than proposed by Anthes, Eq. (12). The consequences on calculated fatigue lives will be shown later.

Especially for small values of the delay constant, crack arrest occurs. For this case the microstructural length l^* needs to be determined iteratively, in the way that the minimum value of the crack length dependant effective cyclic J-Integral is equal to the threshold value, see Fig. 7 (a). With the identified microstructural length, the delay constant does not need to be recalculated, however, the crack growth constant C_{J} is to be calculated by:

$$C_{\mathrm{J}} = \frac{(a_{\mathrm{end}} + l^*)^{1-m_{\mathrm{J}}} - (a_0 + l^*)^{1-m_{\mathrm{J}}}}{(1 - m_{\mathrm{J}}) \cdot Q} \tag{17}$$

With this step, all parameters are identified to calculate lives under variable amplitude loadings. The input to the algorithm is given by identified hysteresis loops of local stress and strain histories. For cases of local stress concentration, the local stress strain path has to be calculated under consideration of the effective stress concentration factor K_{f}. The procedure consists of the following steps:

1. Calculation of the stabilized crack opening stress according to Newman[44] including modifications[53] for given maximum stress $\sigma_{\max}$ and stress based R-ratio for each load cycle individually:

$$\frac{\sigma_{\mathrm{op}}}{\sigma_{\max}} = \begin{cases} A_0 + A_1 \cdot R + A_2 \cdot R^2 + A_3 \cdot R^3 & \text{for} \quad R \geq 0 \\ A_0 + A_1 \cdot R & \text{for} \quad -2 < R < 0 \\ A_0 - 2 \cdot A_1 & \text{for} \quad R \leq -2 \end{cases} \tag{18}$$

with

$$\mathrm{A}_0 = 0.535 \cos\left(\frac{\pi \cdot \sigma_{\max}}{2 \cdot \sigma_0}\right),$$

$$\mathrm{A}_1 = 0.344 \frac{\sigma_{\max}}{\sigma_0},$$

$$\mathrm{A}_2 = 1 - \mathrm{A}_0 - \mathrm{A}_1 - \mathrm{A}_3,$$

$$\mathrm{A}_3 = 2\mathrm{A}_0 + \mathrm{A}_1 - 1,$$

$$\sigma_0 = \frac{R_{\mathrm{m}} + R'_{\mathrm{p0.2}}}{2}.$$

2. Calculation of the stabilized crack opening/closure strain under constant amplitude loading:

$$\varepsilon_{\mathrm{op,const}} = \varepsilon_{\mathrm{cl,const}} = \varepsilon_{\min} + \frac{\sigma_{\mathrm{op}} - \sigma_{\min}}{E} + 2\left(\frac{\sigma_{\mathrm{op}} - \sigma_{\min}}{2 \cdot K'}\right)^{\frac{1}{n'}} \tag{19}$$

   2.a Calculation of the crack length dependant crack opening/closure strain:

$$\varepsilon^a_{\mathrm{op,const}} = \varepsilon_{\mathrm{cl,const}} - \left(\varepsilon_{\mathrm{cl,const}} - \varepsilon_{\min}\right) \cdot \exp\left((a - a_0)/\Delta a_{\mathrm{ref}}\right). \tag{20}$$

   Store $\varepsilon^a_{\mathrm{op,const}}$ as $\varepsilon_{\mathrm{op,const}}$.

3. Calculation of the crack opening strain for the actual cycle $\varepsilon_{\mathrm{op}}$ depending on the crack opening strain of the previous cycle $\varepsilon_{\mathrm{op,prev}}$:

   Special cases:

   For $\varepsilon_{\max} > \varepsilon_{\mathrm{max,old}}$ or $\varepsilon_{\min} < \varepsilon_{\mathrm{min,old}} \rightarrow \varepsilon_{\mathrm{op}} = \varepsilon_{\mathrm{op,const}}$

   For $\varepsilon_{\max} \leq \varepsilon_{\mathrm{op,prev}} \rightarrow \varepsilon_{\mathrm{op}} = \varepsilon_{\mathrm{op,prev}}$

   Cases with $\varepsilon_{\mathrm{op,const}} \geq \varepsilon_{\mathrm{op,prev}} \rightarrow \varepsilon_{\mathrm{op}} = \varepsilon_{\mathrm{op,prev}}$

   Cases with $\varepsilon_{\mathrm{op,const}} < \varepsilon_{\mathrm{op,prev}}$

   For $\sigma_{\mathrm{a}} \geq 0.4\,\sigma_0 \rightarrow \varepsilon_{\mathrm{op}} = \varepsilon_{\mathrm{op,const}}$

For $\sigma_a < 0.4\,\sigma_0 \rightarrow\ \varepsilon_{op} = \varepsilon_{op,prev}$

4. Calculation of the crack closure stress:

   For $\varepsilon_{op} \leq \varepsilon_{min} \rightarrow \sigma_{cl} = \sigma_{min}$

   For $\varepsilon_{op} > \varepsilon_{min}$, iterative determination of crack closure stress:

$$0 = \varepsilon_{max} - \varepsilon_{op} - \frac{\sigma_{max} - \sigma_{cl}}{E} - 2\left(\frac{\sigma_{max} - \sigma_{cl}}{2 \cdot K'}\right)^{\frac{1}{n'}} \tag{21}$$

5. Calculation of the effective cyclic J-Integral:

$$\Delta J_{eff} = \left[1.24\frac{\Delta\sigma_{eff}{}^2}{E} + \frac{1.02}{\sqrt{n'}}\Delta\sigma_{eff} \cdot \left(\Delta\varepsilon_{eff} - \frac{\Delta\sigma_{eff}}{E}\right)\right] \cdot (a + l^*). \tag{22}$$

   with

$$\Delta\sigma_{eff} = (\sigma_{max} - \sigma_{cl})$$

$$\Delta\varepsilon_{eff} = \left(\varepsilon_{max} - \varepsilon_{op}\right)$$

6. Calculation of the crack length increment Δa and the new crack length a_{new}:

$$\Delta a = \begin{cases} C_J \cdot \left((\Delta J_{eff})^{m_J} - \left(\Delta J_{eff,th}\right)^{m_J}\right) & \text{for } \Delta J_{eff} \geq \Delta J_{eff,th} \\ 0 & \text{for } \Delta J_{eff} < \Delta J_{eff,th} \end{cases} \tag{23}$$

$$a_{new} = a + \Delta a \tag{24}$$

7. Calculation of the left level of the crack opening strain for the next cycle, based on the stabilized crack opening strain $\varepsilon_{op,const}$, the crack opening strain used for the calculation of the actual P_J-value and the crack length increment Δa:

$$\varepsilon_{op,new} = \varepsilon_{op,const} - \left(\varepsilon_{op,const} - \varepsilon_{op}\right) \cdot \exp(-\Delta a/\Delta a_{ref}) \tag{25}$$

8. For the next cycle, the following parameters have to be checked or replaced:

   If $\varepsilon_{max} > \varepsilon_{max,old} \rightarrow \varepsilon_{max,old} = \varepsilon_{max}$

   If $\varepsilon_{min} < \varepsilon_{min,old} \rightarrow \varepsilon_{min,old} = \varepsilon_{min}$

   and

$$a = a_{new}$$

$$\varepsilon_{op,prev} = \varepsilon_{op,new}$$

Steps 1 to 8 are repeated until the crack length reaches the defined criteria for the technical crack length: $a \geq a_{end}$. An overview is given by Fig. 8.

3.2 | Variable temperature

Under an additional loading by variable temperatures, the crack growth parameters have to be identified for some temperatures. Under the assumption that the change of temperature for one cycle is small (e.g. $\Delta T < 10K$), the mean temperature of each cycle can be taken for the damage calculation. For the range between ambient temperature and 350°C, the strain life

curves of the material under investigation differ only in the HCF region. Depending on this constraint and the relation given by Eq. (7), the following expression describes the relation between the crack growth exponent m_J and the Ramberg-Osgood exponent n':

$$m_\mathrm{J}(T) \cdot \left(1 + n'(T)\right) = \mathrm{const.}. \tag{26}$$

The crack growth exponent for a given Temperature T depends on the Ramberg-Osgood exponent and the corresponding values for a reference temperature T_ref:

$$m_\mathrm{J}(T) = m_\mathrm{J}(T_\mathrm{ref}) \cdot \frac{\left(1 + n'(T_\mathrm{ref})\right)}{\left(1 + n'(T)\right)}. \tag{27}$$

For the coefficient $Q(T) \cdot \left(P_\mathrm{J}(T, \varepsilon_\mathrm{a})\right)^{-m_\mathrm{J}(T)} = \mathrm{const.}$ the same condition leads to:

$$Q(T) = Q(T_\mathrm{ref}) \cdot \frac{\left(P_\mathrm{J}(T_\mathrm{ref}, \varepsilon_\mathrm{a})\right)^{-m_\mathrm{J}(T_\mathrm{ref})}}{\left(P_\mathrm{J}(T, \varepsilon_\mathrm{a})\right)^{-m_\mathrm{J}(T)}}. \tag{28}$$

These relations are derived for cycles with high stress and strain ranges where these ranges are nearly similar to effective stress and strain ranges. The crack growth constant C_J and the microstructural length l^* have to be identified in the same way as under constant temperature. A constant value for the chosen initial crack length a_0 is the only condition which need to be fulfilled.

The damage parameter D_TMF [31–35] calculated with temperature dependant material parameters, uses an effective cyclic J-Integral related to crack length and temperature dependant value of $R'_\mathrm{p0.1}$. Within this concept, crack growth coefficient and crack growth exponent keep constant. For the damage parameter P_J calculated with temperature dependant material parameters this kind of temperature dependency can easily be done by:

$$P_\mathrm{J}(T_\mathrm{ref}) = P_\mathrm{J}(T) \cdot \frac{R'_\mathrm{p0.1}(T_\mathrm{ref})}{R'_\mathrm{p0.1}(T)}. \tag{29}$$

This approach was used to make PJ-Orig temperature dependant. Used parameters of resistance side were taken from reference temperature T_ref. This led to the consequence of inconsistencies in strain Wöhler-curves and endurances limits in contrast to experimental values. Based on those observations, the temperature dependency for PJ-RifoT2 was motivated to avoid those inconsistencies and performed as shown above.

4 | PARAMETER IDENTIFICATION

4.1 | PJ-based concepts

The parameters are presented in Tab. 1. Resulting strain Wöhler-curves for both concepts are compared to results under constant amplitude loadings by Fig. 9. Differences of the crack growth exponent lead to different slopes of strain Wöhler-curves. For calculations under variable temperature, with temperatures above and below 180°C, two additional supporting points

were added at 20°C and 350°C. For these temperatures, Ramberg-Osgood-Parameters were estimated following previous investigations[54]. The endurance limit was estimated as $\sigma_{\mathrm{D}} = 0.43 \cdot R_{\mathrm{m}}$ where the factor 0.43 is the same at 180°C.

Tab. 1 shows two parameter-sets for PJ-RifoT2. The first one bases on the delay constant published by Anthes[15] (Eq. (12)), the second one (Eq. (13)) bases on the work of the author[19]. For the second, crack arrest occurs.

3.2 | Further concepts

In addition to calculations with PJ-Orig and PJ-RifoT2, calculations with models based on the damage parameter Z_{D}[36] were performed[19]. Some codes, e.g. KTA 3201.2[1,55] or the ASME Code Section VIII[2], use only Wöhler-curves for strain ranges without considering load sequence and mean stress effects. Therefore, calculation results are presented for comparison based on by the strain-life curve of Langer[56] or the according to the equation of Manson[57]-Coffin[58] and Basquin[59] proposed by Morrow[60]:

$$\varepsilon_{\mathrm{a}} = \varepsilon_{\mathrm{a}}^{\mathrm{el}} + \varepsilon_{\mathrm{a}}^{\mathrm{pl}} = \frac{\sigma_f'}{E} \cdot (2 \cdot N)^b + \varepsilon_f' \cdot (2 \cdot N)^c. \tag{30}$$

Compatibility conditions with the Ramberg-Osgood parameters are considered:

$$n' = \frac{b}{c}, \tag{31}$$

$$K' = \frac{\sigma_f'}{\left(\varepsilon_f'\right)^{n'}}.$$

A further possibility based on this description, is to consider the mean stress according to Smith, Watson and Topper[61]: Within the FKM guideline nonlinear[11], a modified Smith-Watson-Topper damage parameter is used by the work of Bergmann[62] taking the mean stress sensitivity into account. Both damage parameters:

$$P_{\mathrm{SWT}} = \sqrt{(\sigma_{\mathrm{a}} + \sigma_{\mathrm{m}}) \cdot \varepsilon_{\mathrm{a}} \cdot E} \text{ for Smith-Watson-Topper,} \tag{32}$$

$$P_{\mathrm{B}} = \sqrt{(\sigma_{\mathrm{a}} + \sigma_{\mathrm{m}} \cdot k) \cdot \varepsilon_{\mathrm{a}} \cdot E} \text{ for Bergmann,} \tag{33}$$

Share same damage parameter Wöhler-curve:

$$P_{\mathrm{SWT}} = P_{\mathrm{B}} = \sqrt{\sigma_f' \cdot (2 \cdot N)^{2 \cdot b} + \sigma_f' \cdot \varepsilon_f' \cdot E \cdot (2 \cdot N)^{b+c}}. \tag{34}$$

The derived parameters for this Wöhler-curves are given in Tab. 1 as well as the used Bergmann-parameter k distinguishing between positive and negative mean stress as in the FKM-guideline nonlinear[11]. For calculations of fatigue lives of tests under variable amplitude loading, the life-curves of 180°C were used. No endurance limit was specified when applying Eq. 32 or Eq. 36.

5 | RESULTS

Calculated fatigue lives in contrast to the experimentally ones are shown in Tab. 2. All 124 tests under variable amplitude loading were statistically evaluated using the estimated probability by Rossow[63]. The statistical values include the mean value $P_{50\%}$, the scattering $1/T_{10\%/90\%}$ by ratio of probability values of 90% to 10% as well as the minimum and maximum values and their scattering. Calculations based on three different kinds of input-data:

1. Predefined strain histories
2. Applied strain histories including deviations by control of servohydraulic testing machine based on one representative load spectrum at half lifetime
3. Applied load histories including deviations by control of servohydraulic testing machine and relative correction of mean stresses by measurements (including cyclic plastic deformation behaviour) of the material based on one representative load spectrum at halt lifetime, for notch and weld specimens nominal stress histories were taken

Fig. 10 includes a selection of the last two possibilities of input-data. In total, the P_{J}-based concepts show a higher quality of the prediction with increasing accuracy of the input-data. This is not observed for the calculations based on strain ranges by Manson-Coffin and Basquin (MCB), Smith-Watson-Topper (SWT) or the damage Parameter by Bergmann. Best results are achieved in this group by the damage parameter of Bergmann followed by the consideration of pure strain ranges with MCB. In average, these calculations predict too high lifetimes with more than a factor of 2. Calculated results with the presented model PJ-RifoT2 are showing a very good agreement with the experimental results under variable amplitude loading. Especially under consideration of an improvement by the delay constant. In contrast to the results achieved with the original P_{J}-concept, the scattering of the ratio of calculated to experimental number of cycles to failure can be reduced from at least $1/T_{10\%/90\%} = 2.98$ to $1/T_{10\%/90\%} = 2.04$. To evaluate the quality of the achieved results, the scattering of the results under variable amplitudes is compared to the scatter of experimental results under constant amplitude loading, s. Fig. 11. The shown scatter in the direction of fatigue life T_{N} bases on the calculated scatter in the direction of loading T_{N}. Shifting the derived Wöhler-curve according to scattering in load direction leads to the shown scattering in direction of fatigue life, which increases with higher number of cycles in the range of HCF and the transition to endurance limit.
Within the scatter bands of 90% to 10% and 95% to 5% - in each case derived from constant amplitude loading tests - are lying 86% and 92% of the results under variable amplitude loading. This leads to the conclusion that the quality of the prediction under variable amplitude loading is in the order as the scattering of experimental results under constant amplitude loading. There is no option for further improvements unless enabling the prediction of scatter itself, e.g. taking the influence of ramdomly arranged microstructure explicitly into account.

6 | DISCUSSION

6.1 | General

Based on the local concept generally and on the original P_J-concept more particularly, further variants were developed for damage assessment based on short crack growth. One of those developed variants has been presented in this paper: PJ-RifoT2. In contrast to the original P_J-concept, the modifications, extensions and improvements can be summarized:

- Transformation from a damage accumulation to a crack growth calculation
- Substitution of the crack growth law,
- Transformation of short crack threshold behaviour on crack growth itself,
- Optimization of parameter identification,
- Modification of crack opening strains delay behaviour,
- Consideration of transient crack closure,
- Consideration of temperature dependency.

6.2 | Transformation from a damage accumulation to a crack growth calculation

In the P_J-concept, the damage sum of the second run of the load spectrum was extrapolated to all possible further runs. The crack growth calculation resigns these simplifications. Therefore, even load cycles influence to crack opening strain, which damage first time after two runs through the load spectrum. This improvement, by running repeatedly through the load spectrum until the failure criterion ($a = a_{\mathrm{end}}$) is reached, ensures that the calculated fatigue lives are independent whether the load spectrum is defined as a multiple of an original load spectrum or not. Furthermore, it is possible to identify the exact load cycle which leads to the failure. When the load spectrum is applicable only a few times, the resulting difference in calculated runs through the load spectrum can be significant.

6.3 | Substitution of the crack growth law

By replacing Eq. (2) by Eq. (3), the discontinuity in crack growth rate at the threshold is avoided. As a consequence, derived life-curve smoothly approaches the fatigue limit without a kink. However, a unique relation between crack length and the damage sum $\sum n/N$ does no longer exist (Eq. (5). Instead, it is from now on depending on the load level. Consequently, a new load sequence effect is accounted for in the calculation. For example, this means under a multiple step loading, that a higher damage sum $D = \sum n_i/N_i$ can be achieved when smaller cycles are applied at first instead of higher cycles. In reverse order of load application, the expected damage sum will be lower, see Fig. 12 (a).

6.4 Transformation of short cracks threshold behaviour on crack growth itself

The transformation of short crack threshold behaviour on crack growth itself is necessary due to the consideration of the threshold value in the crack growth law. In consideration of the microstructural length l^* on the load side (increased stress intensity at crack tip by fictive extension of the crack length) and not on the resistance side (reduced threshold value) offers several advantages. On the one hand, the identification of the parameters is much easier caused by a constant threshold value which effects that all essential parameters can mainly be identified analytically. On the other hand, it is possible to start crack growth calculations with an initial crack length of $a_0 = 0$. If, however, the crack growth constant C_J is predefined or the initial crack length is freely chosen, even under variable amplitude loading there is no change in calculated fatigue life.

6.5 | Modified delay behaviour of crack opening strains

With the modified delay behaviour of crack opening strains, the behaviour was coupled to the crack length increments. Contrary to coupling to damage sum contributions, the delay behaviour is slower for shorter cracks than for longer ones. This leads to a further load sequence effect. For the example of a single overload, the influence of the crack length dependant delay behaviour can be explained, see Fig. 12 (b). For long cracks and fast crack growth, the small cycles are less damaging because the state of stabilized crack closure is approached faster than for short cracks and slow crack growth.

6.6 | Transient crack closure behaviour

The developed equation for transient crack closure behaviour (crack length dependant crack closure strain under constant amplitude loading) distinguishes from Anthes[15] formulation. The crack length a is replaced by the increase of the crack length $(a - a_0)$. With this difference, cracks are fully open even for initial crack lengths $a_0 > 0$. In contrast to Anthes calculated delay constants (which was also adopted to FITNET Fitness-for-Service (FFS) – Procedure[64]), the determined delay constants within the presented procedure are much smaller. This leads even to a much faster changes in the crack closure level. With the developed modification of the delay constant, the scattering in prediction accuracy was reduced by about 50% for this kind of tests[17]. For certain combinations of the delay constants Δa_ref and closure levels, crack arrest can be modelled for amplitudes at the fatigue limit and below. However, cracks grow at amplitudes below the initial fatigue limit, even under pulsating compression. For the case of crack arrest, the microstructural crack length l^*needs to be determined iteratively. Consequently, the dependant parameters have to be recalculated. Crack arrest induced by transient crack closure behaviour is responsible for a further load sequence effect. The fatigue limit is to be understood as a state of crack arrest, see Murakami[65] . A schematic definition of a variable fatigue limit, based on the transient crack closure, is shown by Fig. 12 (c).

6.7 | Temperature dependency

Consideration of temperature dependency was done by providing strain Wöhler-curves in the temperature range of interest. This avoids inconsistencies in contrast to the damage parameter D_{TMF} [31,33] which considers the load side (by temperature dependant material parameters) independently from the resistance side (by scaling the crack growth constant or alternatively the damage parameter). Neither calculated fatigue lives, nor the fatigue limit can be described over large temperature ranges adequate to experimental findings under constant amplitude loading[17]. The deviations vary depending on the chosen reference temperature and the temperature dependant material parameters itself. Motivated by these facts, a procedure was developed to determine the crack growth constants depending on temperature dependant material parameters and the temperature dependant damaging behaviour under constant amplitude loading. Especially by modifying the crack growth exponent $m_{\mathrm{J}}(T)$, additional load sequence effects result. In its consequence, the relation of the damage sum (n/N) and crack length varies with the temperature. Here again, the result is a nonlinear damage accumulation, see Fig. 12 (d).

6.8 | Comparison to FKM-Guideline Nonlinear

The presented concept as well as the original P_{J}-concept and its applicable version published in the FKM Guideline Nonlinear[11] require as input the evaluated local stress strain paths by a hysteresis cycle count algorithm. The main difference between the presented concept and the FKM Guideline Nonlinear is here, local stress strain paths are calculated with the fatigue notch factor K_{f} (including notch supporting effects) instead of the stress concentration factor K_{t}. Calculated local stresses and strains are smaller, here. Therefore, load sequence effects originating from cyclic plasticity are here smaller, too. In the short crack growth regime, such sequence effects tend to reduce fatigue life. Smaller sequence effects result in longer calculated lives.

6.9 | Summarizing load sequence effects

Load sequence effects are considered by the local strain approach and the original P_{J}-concept due to:

- mean stress rearrangement by different load ratios from nominal to local,
- plasticity induced crack closure,
- descending fatigue limit.

Additional load sequence effects introduced here are due to:

- substitution of crack growth equation with transformation of short cracks threshold behaviour on crack growth itself,

- crack length dependant delay of crack closure strain,
- transient crack closure behaviour and
- temperature dependency.

Whether or not an effect is more important than another one depends on the load level, material behaviour and many other influencing parameters. Furthermore, the individual effects interact and influence each other.

6.10 | Application for other materials and possible extensions of the model

The extensive experimental investigations of various specimen geometries and load sequences form are a well suited data basis for validating any life prediction concept. It was shown, that the cyclic deformation behaviour under constant amplitude loading of the steel X6CrNiNb18-10 is characterized by a significant Non-Masing-behaviour, further effects of cyclic hardening and softening are observable. Under strain controlled variable amplitude loadings with load ratios different from -1, an additional mean stress relaxation is observed. Taking this mean stress relaxation into account for damage calculation leads to an improved quality of lifetime prediction. Another aspect, which has not been considered in damage calculation, is the cyclic hardening and softening due to plastic deformation, the calculations were done with idealized and stabilized cyclic material parameters neglecting Non-Masing-Behaviour. A so far neglected effect of cyclic hardening is an increase of the fatigue limit due to smaller plastic deformations.

No additional input parameters for the developed concept are needed in contrast to the original P_J-concept, this is one big advantage. For constant temperature, just a strain-life-cure, cyclic Ramberg-Osgood parameters, Young's modulus und ultimate tensile strength are needed. Under variable temperature, these parameters need to be described temperature dependant. The notch effect was just processed as a problem of transferability between unnotched and notched specimens. Whether an explicit consideration of the stress gradient, for example done by Dankert[66], may lead to additional improvements in the quality of lifetime prediction, awaits investigation. Especially in combination with transient crack closure, it could result in a new dynamic of the crack arrest. With the consequences of a new assessment of the fatigue limit of notched bodies in contrast to unnotched bodies. In this context it will also be required to review the applied method of the statistical support effect.

For thermo-mechanical loading a reference temperature must be defined and the equation for the effective cyclic J-Integral has to be replaced, for example according to Bauerbach, Schlitzer and co-authors[54,67,68].

Future developments should focus on the modelling of the transient cyclic deformation behaviour. Such a modelling must be fast and efficient, against the background of several millions of cycles. Therefore, extensive FE-calculations are excluded explicitly. During the investigations,

only the mean stress relaxation in the nominal section of the notched specimens was considered for damage calculations. Locally in the notch, the effect of mean stress relaxation differs from behaviour in the nominal section and is additionally combined with ratcheting, for example shown by Panic[69]. The consideration of an additional mean stress relaxation combined with ratcheting in the notch is expected to provide improved fatigue assessment results.

7 | CONCLUSION

The presented model is an improvement and extension to the original P_J-model. Substitution of the damage accumulation by crack propagation leads to new possibilities in the extension of the original model. Additional sequence effects are considered by the transient and crack length dependant crack closure formulation, the improved threshold behaviour and even the temperature dependent crack growth exponent. These additional sequence effects led to the consequence that the scatter of ratios of calculated and experimentally determined lives under variable amplitude is comparable to the scatter under constant amplitude loading.

ACKNOWLEDGEMENTS

Experimental findings were achieved within the IGF-project 18.842 N “Erweiterte Schädigungskonzepte für thermomechanische Beanspruchung unter variablen Amplituden und plastischer Deformation“ of the research association “Schweißen und verwandte Verfahren e.V.” of the DVS, Aachener Str. 172, 40223 Düsseldorf and funded by the AiF within the scope of the program for advancement of the industrial alliance of research (IGF) of the Federal Ministry for Economic Affairs and Energy on the basis of a decision by the German Bundestag. The financial support is greatly acknowledged. The research project was done together with Sophie Schackert and Christoph Schweizer from Fraunhofer Institute for Mechanics of Materials IWM, Freiburg, Germany. A majority of experimental results were achieved in Freiburg. We would like to thank them for the good and productive collaboration.

ORCID

A. Bosch https://orcid.org/0000-0002-0954-443X

M. Vormwald https://orcid.org/0000-0002-4277-785X

REFERENCES

1. KTA 3201.2. Komponenten des Primärkreises von Leichtwasserreaktoren Teil 2: Auslegung, Konstruktion und Berechnung.2013.
2. ASME Boiler, Pressure Vessel Code Section VIII Division 2. Alternative Rules, Rules for Construction of Pressure Vessels.2007.
3. Palmgren A. Die Lebensdauer von Kugellagern. VDI-Z 1924;68(14):339–41.

4. Miner MA. Cumulative Damage in Fatigue. Transactions of ASME, Journal of Applied Mechanics 1945;12(6):359-365.
5. Vormwald M. Classification of Load Sequence Effects in Metallic Structures. Procedia Engineering 2015;101:534–42.
6. Fatemi A, Yang L. Cumulative fatigue damage and life prediction theories: a survey of the state of the art for homogeneous materials. Int. journal of fatigue 1998;20(1):9–34.
7. Skorupa M. Load interaction effects during fatigue crack growth under variable amplitude loading - A literature review. Part I: Empirical trends. Fatigue Fract. Engng. Mater. Struct. 1998;21(8):987–1006.
8. Skorupa M. Load interaction effects during fatigue crack growth under variable amplitude loading-a literature review. Part II: qualitative interpretation. Fatigue Fract. Engng. Mater. Struct. 1999;22(10):905–26.
9. Dowling NE. 4.03 - Local Strain Approach to Fatigue. In: Ritchie RO, editor. Comprehensive Structural Integrity. Oxford: Pergamon.2003, p. 77–94.
10. Fiedler M, Vormwald M. Considering fatigue load sequence effects by applying the Local Strain Approach and a fracture mechanics based damage parameter. Theoretical and Applied Fracture Mechanics 2016;83:31–41.
11. Fiedler M, Wächter M, Varfolomeev I, Vormwald M, Esderts A. Richtlinie Nichtlinear: Rechnerischer Festigkeitsnachweis unter expliziter Erfassung nichtlinearen Werkstoffverformungsverhaltens für Bauteile aus Stahl, Stahlguss und Aluminiumknetlegierungen. 1st ed. Frankfurt am Main: VDMA Verlag GmbH.2019.
12. Vormwald M, Seeger T. The Consequences of Short Crack Closure on Fatigue Crack Growth Under Variable Amplitude Loading. Fatigue and Fract. Engng. Mater. Struct. 1991;14(2/3):205–25.
13. Vormwald M, Heuler P, Seeger T. A Fracture Mechanics Based Model for Cumulative Damage Assessment as Part of Fatigue Life Prediction. In: M.R. Mitchell, R.W. Landgraf, editors. Advances in Fatigue Life Prediction Techniques, San Francisco. Philadelphia.1992, p. 28–46.
14. Vormwald M, Heuler P, Krä C. Spectrum Fatigue Life Assessment of Notched Specimens Using a Fracture Mechanics Based Approach. In: H. Amzallag, (Ed.), Automation in Fatigue and Fracture Testing and Analysis, ASTM STP 1231 1994:219–31.
15. Anthes RJ. Ein neuartiges Kurzrißfortschrittsmodell zur Anrißlebensdauervorhersage bei wiederholter Beanspruchung. Report 57: Inst. f. Stahlbau und Werkstoffmechanik, TH Darmstadt.1997.
16. Bosch A, Vormwald M. Concepts for crack propagation under variable mechanical and thermal loadings based on the effective cyclic J-Integral. In: Decker M, editor. VAL4 -

Fourth International Conference on Material and Component Performance under Variable Amplitude Loading. Berlin: DVM.2020, p. 323–332.
17. Schackert S, Bosch A, Schweizer C, Vormwald M. Erweiterte Schädigungskonzepte für thermomechanische Beanspruchung unter variablen Amplituden und plastischer Deformation. Report AiF-No. 18.842.2018.
18. Schackert S, Schweizer C, Vormwald M, Bosch A. Lebensdauerbewertung geschweißter Rohrleitungen aus dem austenitischen Stahl 1.4550 mithilfe von Kurzrisswachstumsmodellen. Schweißen und Schneiden 2019(5):286–92.
19. Bosch A. Kurzrisswachstumsmodelle unter Berücksichtigung variabler strukturmechanischer und thermischer Belastung. Report 127: Inst. f. Stahlbau u. Werkstoffmechanik, TU Darmstadt.2019.
20. Smaga, Boemke, Daniel, Skorupski, Sorich, Beck. Fatigue Behavior of Metastable Austenitic Stainless Steels in LCF, HCF and VHCF Regimes at Ambient and Elevated Temperatures. Metals 2019;9(6):704.
21. Bayerlein M, Christ H-J, Mughrabi H. Plasticity-induced martensitic transformation during cyclic deformation of AISI 304L stainless steel. Materials Science and Engineering: A 1989;114:L11-L16.
22. Neuber HH. Theory of Stress Concentration for Shear-Strained Prismatical Bodies With Arbitrary Nonlinear Stress-Strain Law. Journal of Applied Mechanics 1961;24(4):544–50.
23. Ramberg W, Osgood W. Description of stress-strain curves by three parameters.1943.
24. Finney DJ. Probit analysis. In: London: Cambridge University Press.1947.
25. Lemaitre J, Chaboche J-L. Mechanics of solid materials. Cambridge University Press.1990.
26. Döring R. Zum Deformations- und Schädigungsverhalten metallischer Werkstoffe unter mehrachsig nichtproportionalen zyklischen Beanspruchungen. Report 57: Inst. f. Stahlbau und Werkstoffmechanik, TU Darmstadt.2006.
27. Fang J. Cyclic plasticity modelilng and multiaxial fatigue assessment for an austenitic steel. München: Herbert Utz Verlag GmbH.2015.
28. Bosch A, Vormwald M. Rissfortschrittskonzepte auf Grundlage des effektiven zyklischen J-Integrals für Strukturen unter variabler strukturmechanischer und thermischer Belastung. In: 51. Tagung des Arbeitskreises Bruchmechanik und Bauteilsicherheit. Berlin: DVM.2019, p. 137–148.
29. Bosch A, Schackert S, Schweizer C, Vormwald M. Fatigue Life of Welded Joints of AISI 347 Stainless Steel Under Thermomechanical and Variable Amplitude Loading. In: Proc. of the ASME Pressure Vessels and Piping Conference.2018, V03BT03A007.
30. Bosch A, Schackert S, Schweizer C, Vormwald M. Fatigue life assessment of welded joints made of the stainless steel X6CrNiNb18-10 for thermomechanical and variable amplitude loading. Materials science and engineering technology 2018;49(3):316–31.

31. Riedel H. Fracture at High Temperatures. Springer-Verlag, Berlin, Heidelberg, New York.1987.
32. Maier G, Möser M, Riedel H, Seifert T, Siegele D, Klöwer J et al. High Temperature Plasticity and Damage Mechanisms of the Nickel Alloy 617B. In: Proc. of the 36th MPA-Seminar Materials and Components Behaviour in Energy & Plant Technology.2010.
33. Schmitt W, Mohrmann R, Riedel H, Dietsche A, Fischersworring-Bunk A. Modelling of the fatigue life of automobile exhaust components. In: Proc. of the 8th International Fatigue Congress.2002, p. 781–788.
34. Seifert T, Schweizer C, Schlesinger M, Möser M, Eibl M. Thermomechanical fatigue of 1.4849 cast steel – experiments and life prediction using a fracture mechanics approach. IJMR (Int. Journal of Materials Research) 2010;101(8):942–50.
35. Schweizer C, Seifert T, Nieweg B, Hartrott P von, Riedel H. Mechanisms and modelling of fatigue crack growth under combined low and high cycle fatigue loading. Int. journal of fatigue 2011;33(2):194–202.
36. Heitmann HH, Vehoff H, Neumann P. Random Load Fatigue of Steels: Service Life Prediction Based on the Behaviour of Microcracks. In: Proc. of the International Conference 1983.
37. Heitmann HH. Betriebsfestigkeit von Stahl: Vorhersage der technischen Anrißlebensdauer unter Berücksichtigung des Verhaltens von Mikrorissen: Fak. für Bergbau und Hüttenwesen, RWTH Aachen.1983.
38. Kamaya M, Kawakubo M. Loading sequence effect on fatigue life of Type 316 stainless steel. Int. journal of fatigue 2015;81:10–20.
39. Liang W, Conle FA, Topper TH, Walbridge S. A review of effective-strain based and multi R-ratio crack propagation models and a comparison of simulated results using the two approaches. Int. journal of fatigue 2021;142:105920.
40. Vormwald M. Anrißlebensdauervorhersage auf der Basis der Schwingbruchmechanik für kurze Risse. Report 47: Inst. f. Stahlbau und Werkstoffmechanik, TH Darmstadt.1989.
41. Dowling NE. J-integral estimates for cracks in infinite bodies. Eng. Frac. Mech. 1987;26(3):333–48.
42. El Haddad MH, Dowling NE, Topper TH, Smith KN. J integral applications for short fatigue cracks at notches. Int. Journal of Fracture 1980;16(1):42–6.
43. Tanaka K, Nakai Y, Yamashita M. Fatigue growth threshold of small cracks. Int. journal of fatigue 1981;17(5):519–33.
44. Newman Jr. JC. A crack opening stress equation for fatigue crack growth. Int. Journal of Fracture 1984;24:R131-R135.
45. Ebi G G, Riedel H, Neumann P. Fatigue life prediction based on microcrack growth. Proc. 6th European Conf. Fracture 1986:1587–98.

46. Chopra OK, Shack WJ. Effect of LWR coolant environments on the fatigue life of reactor materials. U.S. Nuclear Regulatory Commission, Office of Nuclear Regulatory Research Washington, DC.2007.
47. Gavenda DJ, Luebbers PR, Chopra OK. Crack initiation and crack growth behavior of carbon and low-alloy steels.1997.
48. Suresh S, Ritchie R. Propagation of short fatigue cracks. Int. Met. Rev. 1984;29:445–76.
49. Dowling NE, Begley JA. Fatigue crack growth during gross plasticity and the J - integral. ASTM590 1976;ASTM STP 590:82 - 103.
50. Gamache B, McEvily AJ. On the development of fatigue crack closure. In: J.-P.Bailon, J.I. Dickson, editors. FATIGUE 93 - Proc. 5th Int. Conf. on Fatigue and Fatigue Thresholds. Montreal, Quebec, Kanada.1993, p. 577–582.
51. P. Heuler. Anrißlebensdauervorhersage bei zufallsartiger Belastung auf der Grundlage örtlicher Beanspruchungen. Report 40: Inst. f. Stahlbau und Werkstoffmechanik, TH Darmstadt.1983.
52. Taylor D. A Compendium of Fatigue Thresholds and Growth Rates. Engineering Materials Advisory Services, Warley.1985.
53. Southwest Research Institute. NASGRO v6.1 Release Notes. San Antonio, Texas.2010.
54. Bauerbach K, Beier HT, Fischaleck M, Rudolph J, Schlitzer T, Scholz A et al. Numerische Simulation und experimentelle Charakterisierung des Ermüdungsrisswachstums unter thermozyklischer Beanspruchung. Report BMBF 02NUK009D H 139457. Darmstadt.2013.
55. Schuler X, Herter K-H, Rudolph J. Derivation of Design Fatigue Curves for Austenitic Stainless Steel Grades 1.4541 and 1.4550 Within the German Nuclear Safety Standard KTA 3201.2. In: Proc. of the ASME Pressure Vessel and Piping Conference.2013.
56. Langer BF. Design of Pressure Vessels for Low-Cycle Fatigue. Journal of Basic Engineering 1962;84(3):389–99.
57. Manson SS. Behaviour of Materials Under Conditions of Thermal Stress. NACA: TN-2993.1953.
58. Coffin Jr. LF. A study of the effects of cyclic thermal stresses on a ductile metal. Transactions of the ASME 1954;76:931–50.
59. Basquin OH. The exponential law of endurance tests. American Society of Testing Materials 1910(10):625–30.
60. Morrow JD. Cyclic Plastic Strain Energy and Fatigue of Metals. In: Internal Friction, Damping, and Cyclic Plasticity. ASTM.1965, p. 45–87.
61. Smith KN, Watson P, Topper TH. A Stress-Strain Function for the Fatigue of Metals. Journal of Materials 1970;5(4):767–78.

62. Bergmann JW. Zur Betriebsfestigkeitsbemessung gekerbter Bauteile auf der Grundlage der örtlichen Beanspruchungen. Report 37: Inst. f. Stahlbau und Werkstoffmechanik, TH Darmstadt.1983.
63. Rossow E. Eine einfache Rechenschiebernäherung an die den normal scores entsprechenden Prozentpunkte. Qualitätskontrolle 1964;9(12):146–7.
64. Koçak, M., Webster, S., Janosch, J.J., Ainsworth, R.A., Koers, R. FITNET Fitness-for-Service (FFS) - Procedure (Vol. 1). 1st ed. GKSS Geesthacht.2008.
65. Murakami Y. Metal Fatigue: Effects Of Small Defects And Nonmetallic Inclusions. Elsevier Ed 2002.
66. Dankert M. Ermüdungsrißwachstum in Kerben - Ein einheitliches Konzept zu Berechnung von Anriß- und Rißfortschrittslebensdauern. Report 60: Inst. f. Stahlbau und Werkstoffmechanik, TU Darmstadt.1999.
67. Schlitzer T, Bauerbach K, Beier HT, Fischalek M, Langschwager K, Oechsner M et al. Experimental characterization and numerical assessment of fatigue crack growth under thermo-mechanical conditions. Mat. -wiss. u. Werkstofftech. 2015;46(2):165–77.
68. Bauerbach K. Numerische Betrachtungen zu Deformationsverhalten und Schädigungsbewertung kurzer Risse unter thermozyklischer Beanspruchung. Report 103: Inst. f. Stahlbau und Werkstoffmechanik, TU Darmstadt.2014.
69. Panic D, Beier TH, Vormwald M. Damage Assessment of Threaded Connections based on an Advanced Material Model and Local Concepts. Procedia Engineering 2014;74:119–28.

Hourglass (HG) specimen (IFSW)	Smooth specimen (IWM)	Notch specimen (IFSW)	Weld specimen (IWM)	Gleeble specimen (IWM)
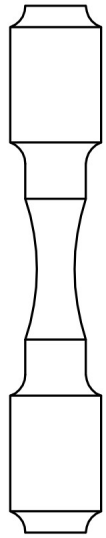	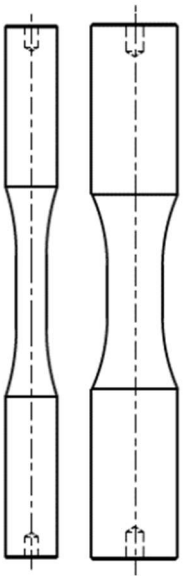	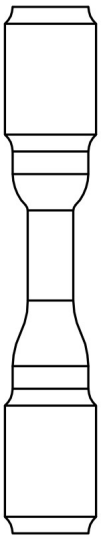	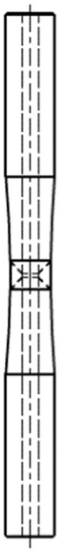	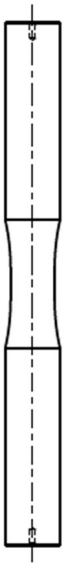
base material	base material	base material	base material/ weld material	heat affected zone (HAZ)
		geometrical notch $r = 1\text{mm}$	metallurgical and geometrical notch $r{\sim}0{,}01\text{mm}$	simulated charac-teristics of HAZ
$d = 5\text{mm}$	$d = 7\text{mm}$ $/(d = 8\text{mm})$	$d = 5{,}5\text{mm}$	$d_1 = 12\text{mm}$ $d_2 = 4\text{mm}$	$d = 8\text{mm}$
$K_\text{t} = 1{,}02$ $K_\text{f}{\sim}1{,}00$	$K_\text{t} = 1{,}00$ $K_\text{f} = 1{,}00$	$K_\text{t} = 1{,}57$ $K_\text{f} = 1{,}26$	$K_\text{t} = 3{,}00$ $K_\text{f} = 1{,}93$	$K_\text{t} = 1{,}00$ $K_\text{f} = 1{,}00$

Fig. 1 Overview of specimen types by geometry, material, special characteristics, diameter in nominal section (for Weld Specimen outer diameter d_1 and diameter of inner drill d_2), stress concentration and effective stress concentration factor used for calculations

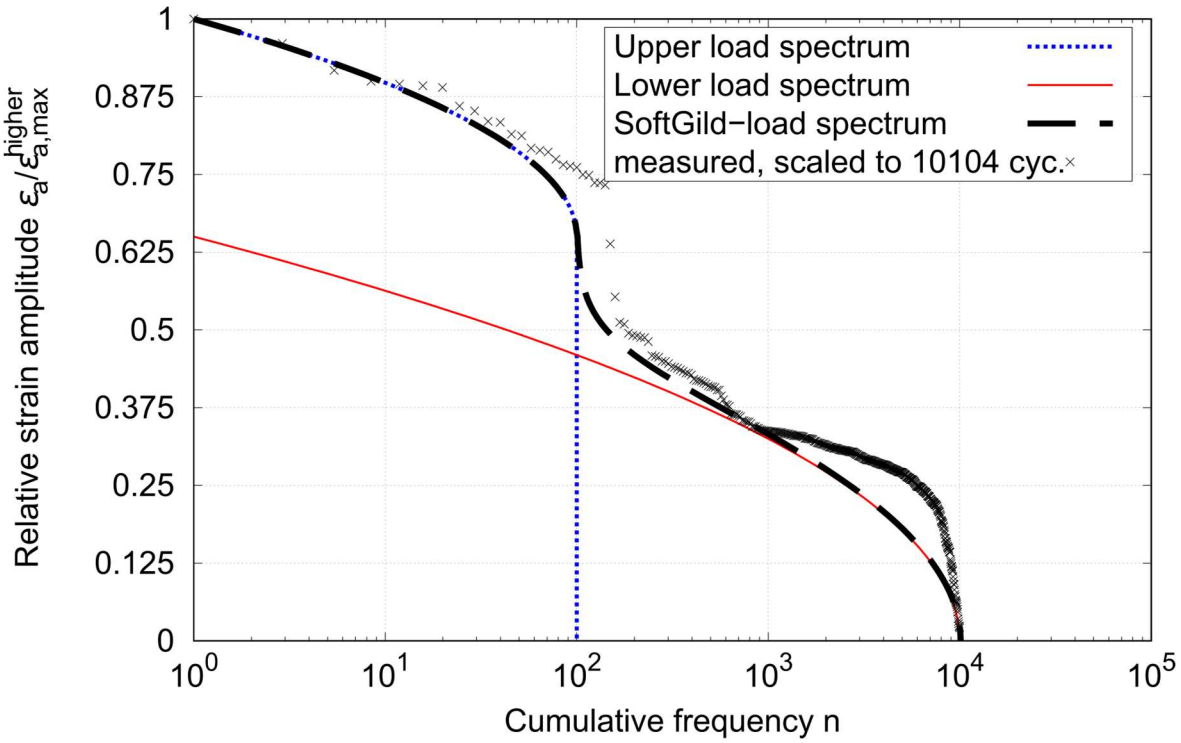

Relative amplitudes and frequencies for derived load spectrum

Step	1.	2.	3.	4.	5.	6.	7.	8.
Relative amplitude $\varepsilon_a/\varepsilon_{a,max}$	1	7/8	6/8	5/8	4/8	3/8	2/8	1/8
Frequency	2	8	40	52	42	650	3490	5820
Cumulative frequency	2	10	50	102	144	794	4284	10104

Fig. 2 Derived load spectra for strain amplitudes, graphical sketch in contrast to measured load spectrum and numbers for step levels and corresponding cycle numbers

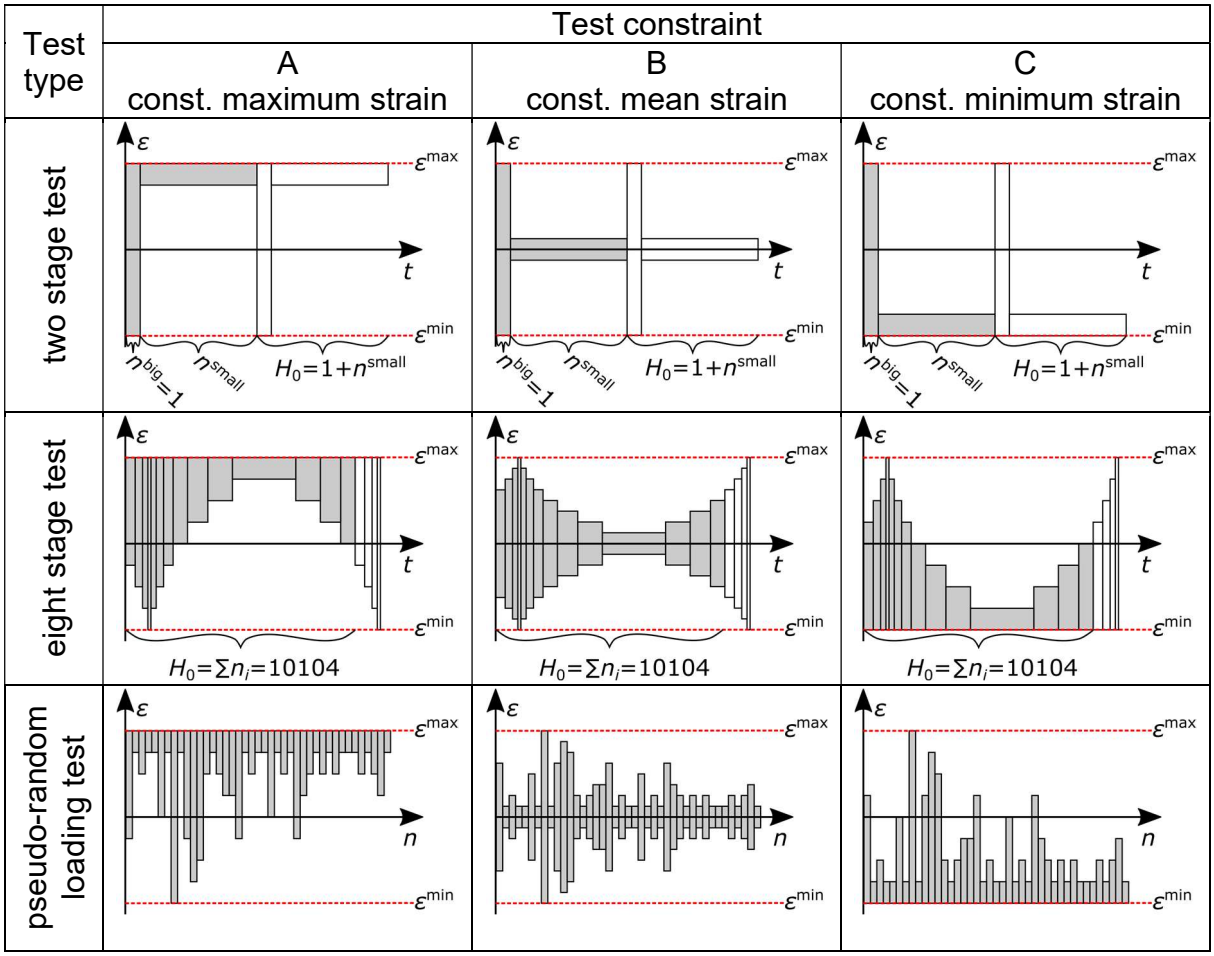

Fig. 3 Schematic illustration of test matrix with two stage tests (first line), eight stage tests (second line) and pseudo-random loading tests (third line); schematic illustration of the pseudo-random loading tests shows just a section of the load spectrum, each bar illustrates one load cycle

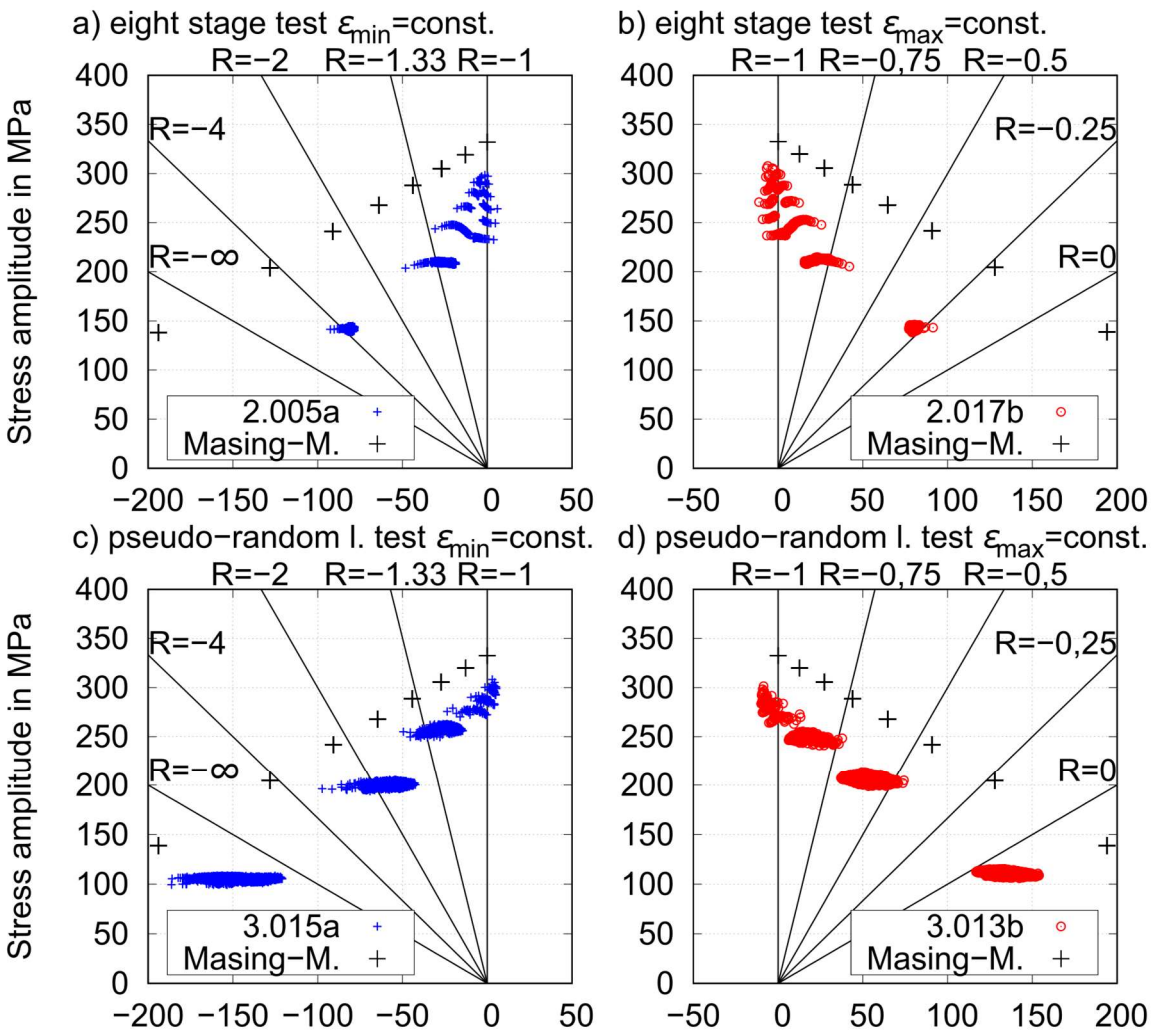

Fig. 4 Resulting mean stresses under variable amplitude strain controlled loading exemplary for two eight stage tests and two operational loading tests, in each case one example with constant minimum strain (left) and one example with constant maximum strain (right) compared to calculations with Masing-Memory-Behaviour based on stabilized behaviour under constant amplitude loading

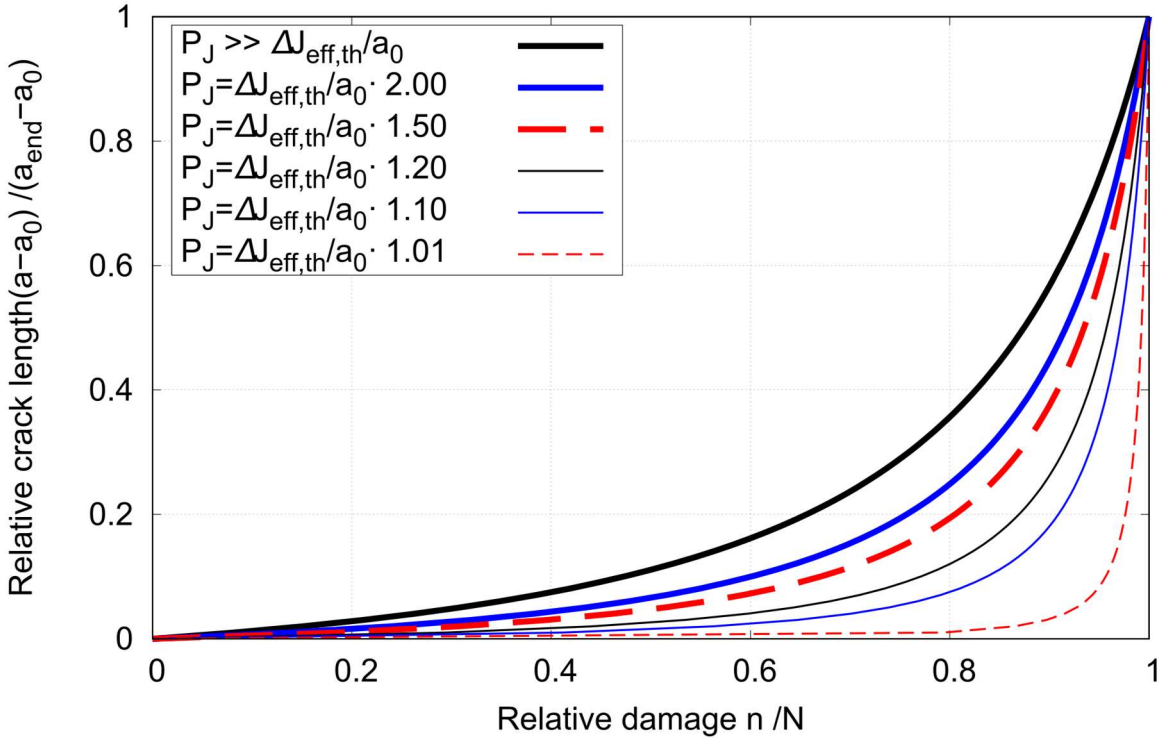

Fig. 5 Relation between relative crack length and relative damage under constant amplitude loading and the assumption of stabilized crack closure behaviour depending on load level relative to threshold

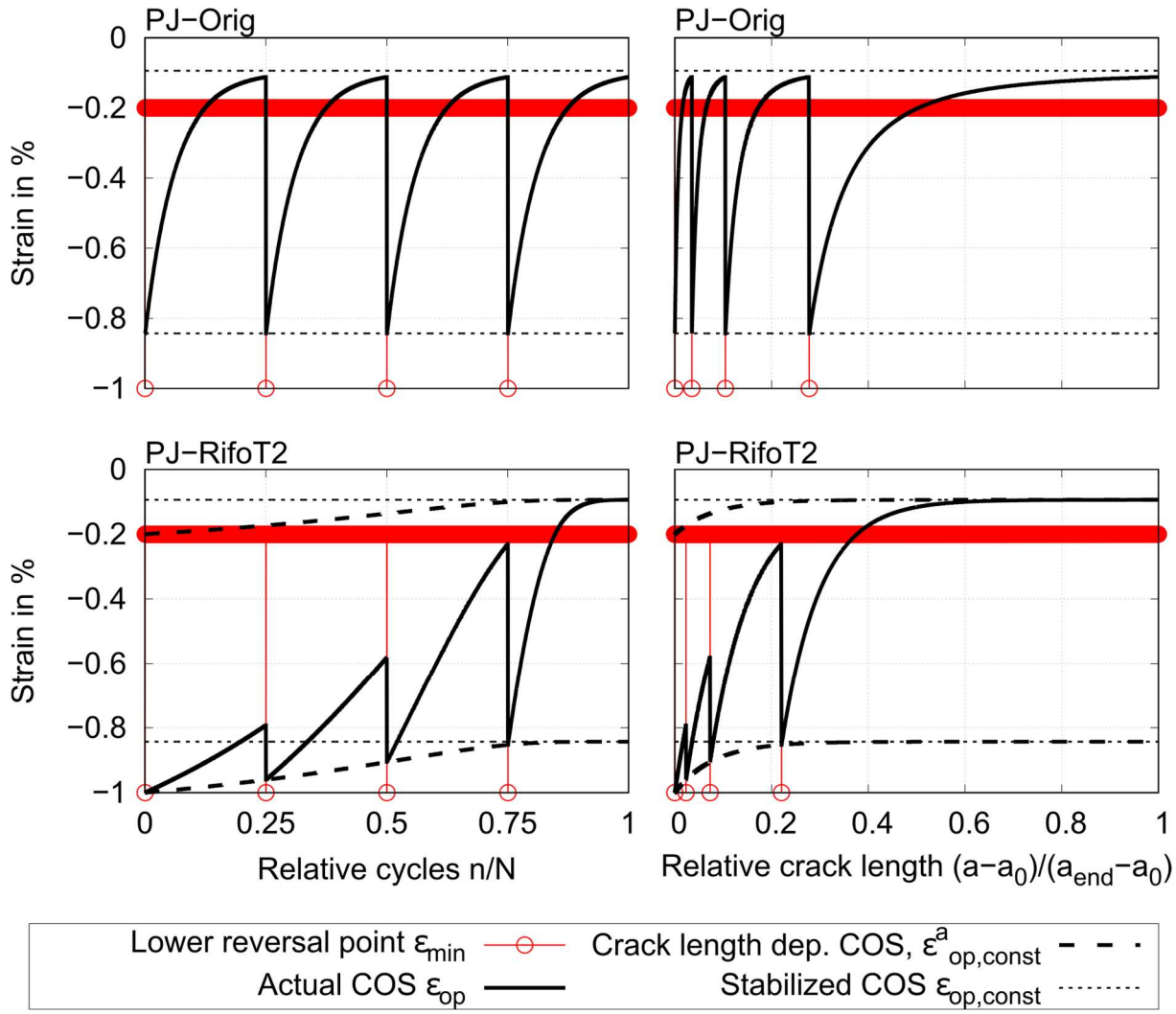

Fig. 6 Schematic behaviour of Crack Closure Strain (COS) for concept PJ-Orig and PJ-RifoT2 for an exemplary two stages test (1 cycle with $\varepsilon_a = 1\%$ under $R_\varepsilon = -1$ followed by a high number of cycles with $\varepsilon_a = 0.2\%$ under $R_\varepsilon = -1$) normalized to 4 repeats, shown over relative cycles (left column) and relative crack length (right column)

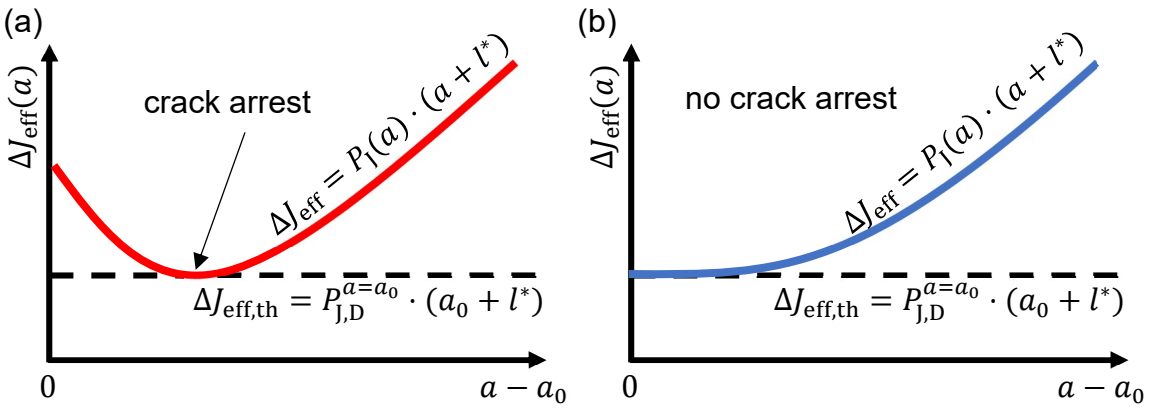

Fig. 7 Example for crack arrest (a) and no crack arrest (b)

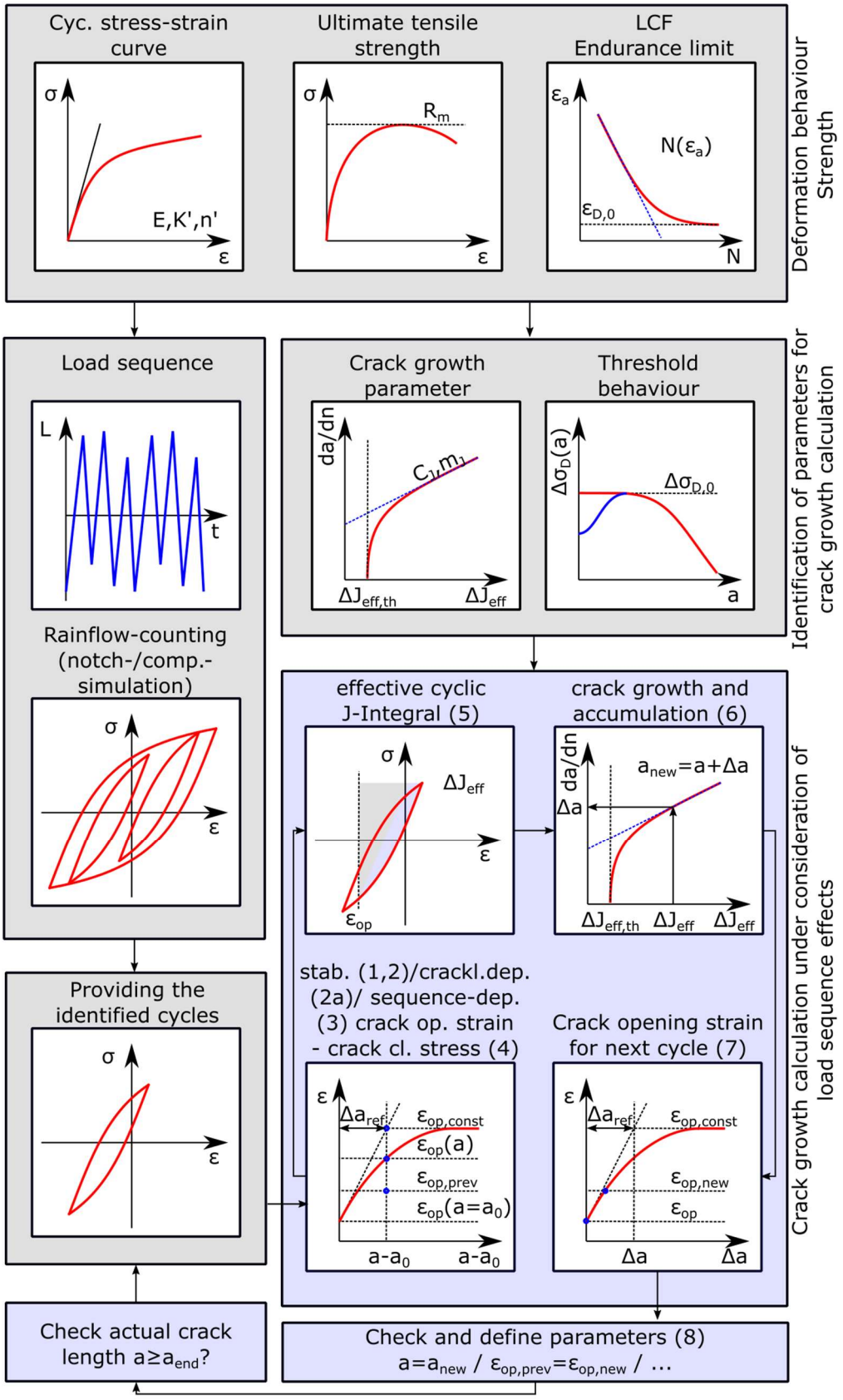

Fig. 8 Overview of the presented procedure for input, identification of parameters, providing the load input and how to perform under variable amplitude loading

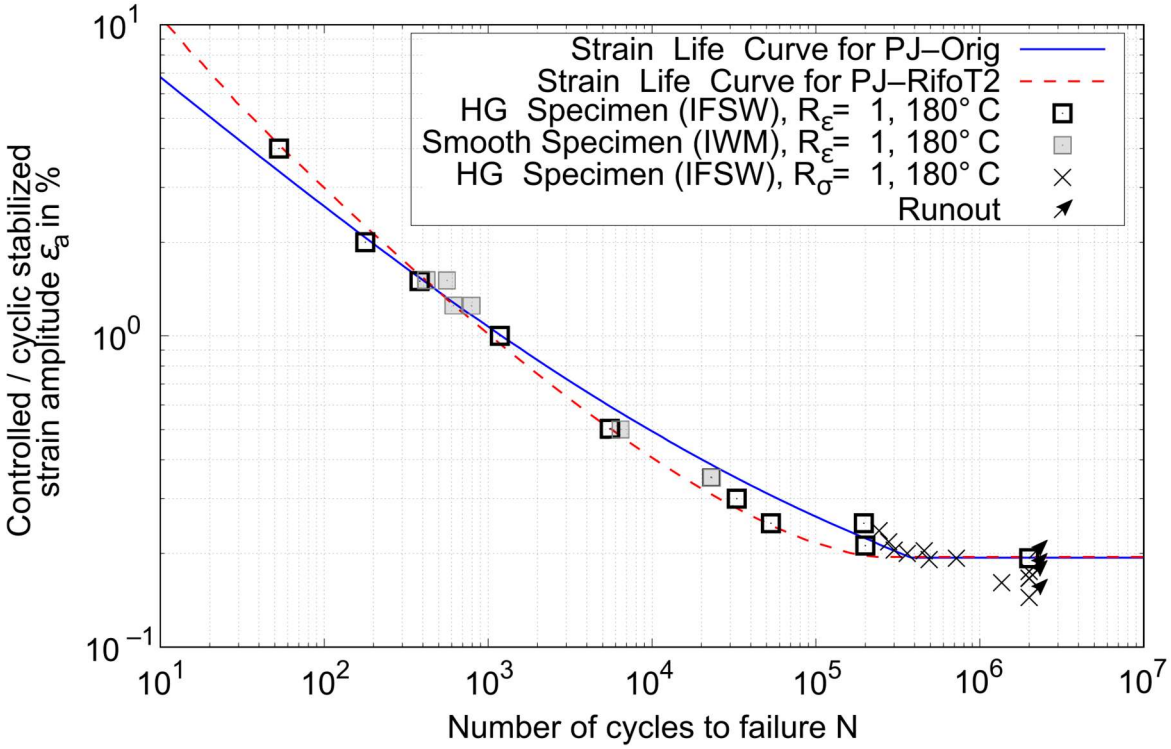

Fig. 9 Comparison of resulting strain-life-curves under constant amplitude loading for PJ-Orig and with improved adjustment for PJ-RifoT2 in contrast to experimental results for HG- and smooth specimens

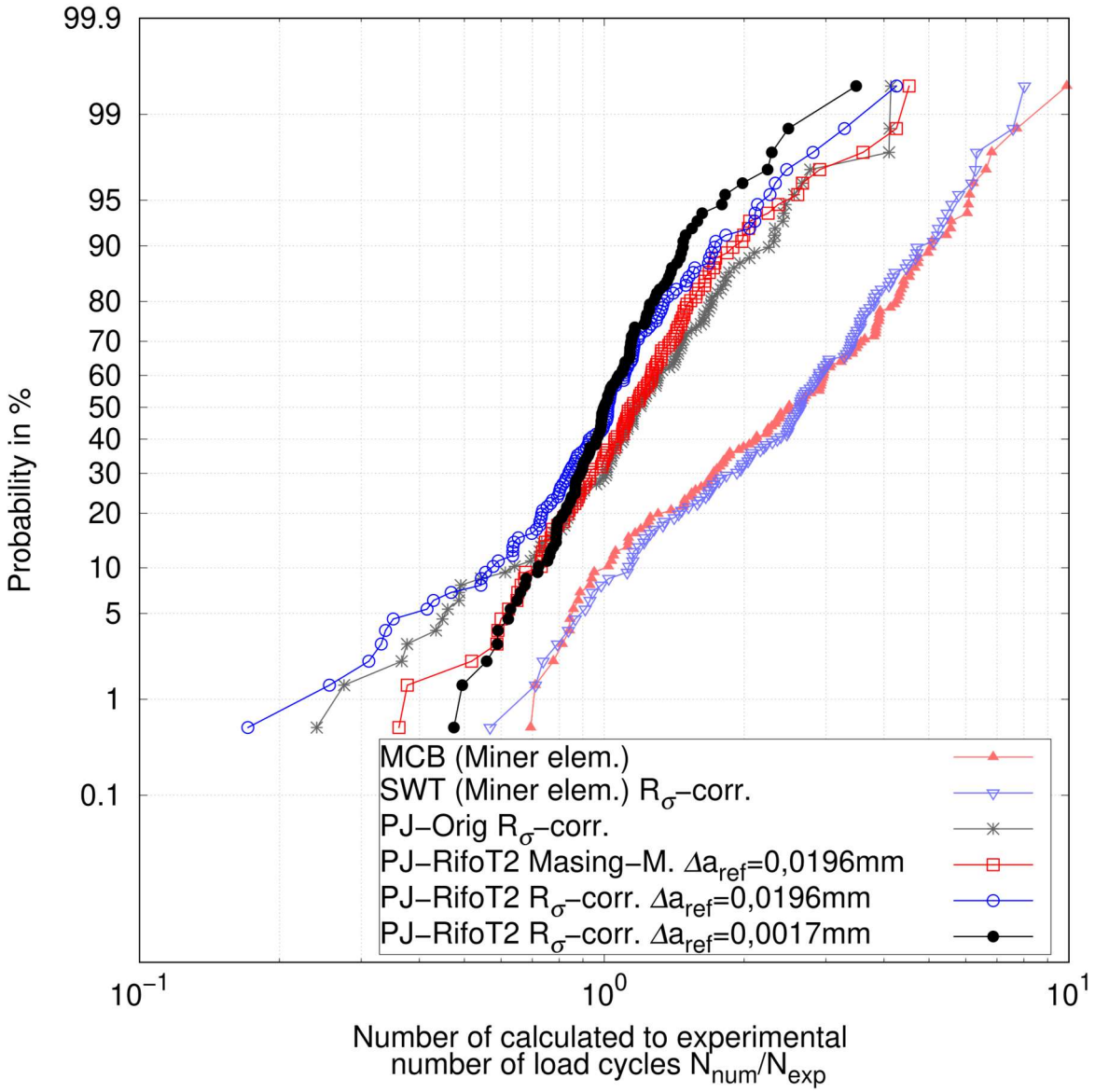

Fig. 10 Comparison of different damage concepts and variations concerning quality of lifetime prediction

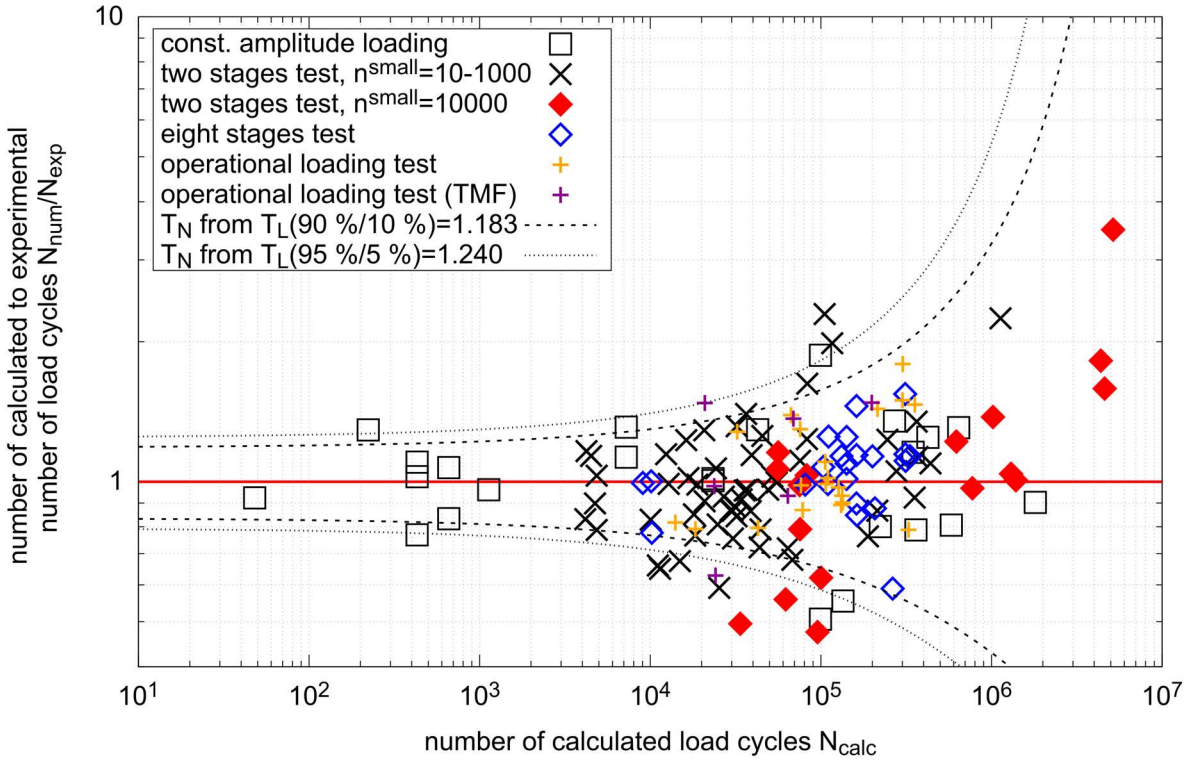

Fig. 11 Comparison of scattering of results under variable amplitude loading to scatter of results under constant amplitude loading

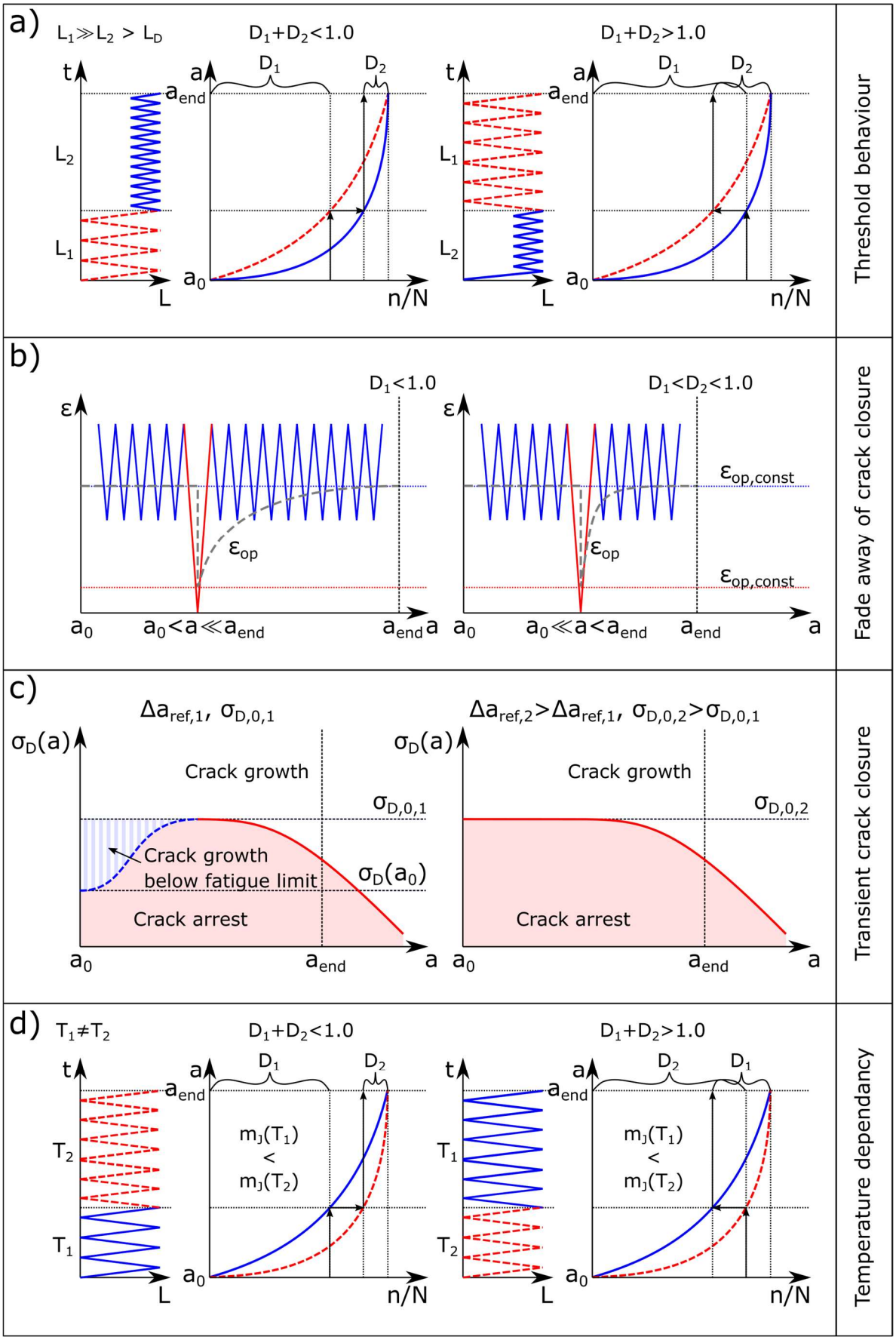

Fig. 12 Illustration of main additional load sequence effects by the developed concept

Tab. 1 Material parameters for X6CrNiNb18-10

a) Results of materials tests

Temp. T in °C	Young's modulus E in °C	Hardening coeff. K' in °C	Hardening exp. n' in °C	Ultimate tensile strength R_m in MPa	Endurance limit* σ_D in °C	Threshold value $\Delta J_\mathrm{eff,th}$ in MPa mm
20	199182	2018	0.2969	675	290	0.0398
180	183000	1121	0.2309	495	214	0.0366
350	172410	793	0.1941	440	190	0.0345

b) Derived model dependant parameters, all values in the dimensions of N and mm, $a_\mathrm{end} = 0.25\ \mathrm{mm}$, indirect parameters in brackets

Model	Parameters					
PJ-Orig	m_J	C_J	Q	l^*	a_0	$P_\mathrm{J,D,0}$
	1.863	0.0000650	509588	0.0133	0.0181	1.167
PJ-RifoT2 based on Eq. (12) with $\Delta a_\mathrm{ref} = 0.0196\ \mathrm{mm}$	m_J	C_J	(Q)	l^*	a_0	$P_\mathrm{J,D}^{a=a_0}$
	1.589	0.0000913	188903	0.0139	0.0	2.636
PJ-RifoT2 based on Eq. (13) with $\Delta a_\mathrm{ref} = 0.0017\ \mathrm{mm}$	m_J	C_J	(Q)	l^*	a_0	$P_\mathrm{J,D}^{a=a_0}$
	1.589	0.0000603	188903	0.0247	0.0	2.636

c) Parameters for describing the strain-life curve and the mean stress sensitivity

Model	Parameters			
Manson-Coffin, Basquin (MCB), Smith-Watson-Topper (SWT) and Bergmann	σ_f'	ε_f'	b	c
	764	0.19025	-0.09391	-4.0671
Bergmann	k for $\sigma_\mathrm{m} \geq 0$		k for $\sigma_\mathrm{m} < 0$	
	0.1519		0.0494	

*reduced for weld- and Gleeble-specimens, see chapter 2.3

Tab. 2 Comparison of calculated and experimentally achieved fatigue lives based on statistical values for several models and type of input-data

Model	Input	$P_{50\%}$	$1/T_{10\%/90\%}$	min	max	max/min
MCB	Predefined strain histories	2.51	4.78	0.65	8.86	13.63
SWT		2.39	8.73	0.19	35.9	188.58
Bergmann		2.35	3.8	0.69	7.66	11.14
PJ-Orig		1.20	3.32	0.21	4.62	21.75
PJ-RifoT2 $\Delta a_{\mathrm{ref}} = 0.0196$ mm		1.07	2.84	0.25	4.70	18.50
MCB	Applied strain histories	2.48	4.97	0.69	9.87	14.22
SWT		2.14	7.08	0.39	37.07	94.52
Bergmann		2.51	4.01	0.70	8.61	12.38
PJ-Orig		1.26	2.98	0.28	7.48	26.99
PJ-RifoT2 $\Delta a_{\mathrm{ref}} = 0.0196$ mm		1.08	2.66	0.36	4.53	12.52
MCB	Applied strain histories, R_σ-corrected	2.43	5.24	0.53	10.43	19.88
SWT		2.64	4.17	0.57	8.02	14.13
Bergmann		2.45	4.58	0.55	9.48	17.18
PJ-Orig		1.16	3.51	0.24	4.14	17.19
PJ-RifoT2 $\Delta a_{\mathrm{ref}} = 0.0196$ mm		0.99	2.75	0.17	4.26	25.00
PJ-RifoT2 $\Delta a_{\mathrm{ref}} = 0.0017$ mm		1.00	2.04	0.48	3.49	7.34